Critical Review -- The Bipolar Trickle Tower Reactor: Concept, Development and Applications

Frank C. Walsh,* Luis F. Arenas, Carlos Ponce de León

Electrochemical Engineering Laboratory, Faculty of Engineering and the Environment,

University of Southampton, Southampton, SO17 1BJ, UK.

* Author for correspondence; f.c.walsh@soton.ac.uk

Abstract

The concept of a trickle tower, using ordered bipolar electrode elements stacked in (10 to 80) similar layers of porous, 3D electrodes separated by insulating separator meshes is described and key features of electrochemical reactors based on the bipolar trickle tower reactor (BTTR) geometry are reviewed. Fluid flow, mass transfer, active area and bypass current are considered in detail, since they affect the reaction environment. Modified reactor designs have resulted from the process of electrode selection and tower construction. The performance of BTTRs is illustrated by examples from laboratory and industry, including electrosynthesis and environmental treatment. Experimental data are used to rationalise reaction environment and simulate performance. Operational factors such as electrolyte flow, mass transport rates and volumetric electrode area are highlighted as important factors in achieving high efficiency; minimisation of internal bypass currents is critical. Developments have enabled improvements in reactor construction and a wider choice of electrode material. Future R & D needs are highlighted.

Keywords: bipolar electrode; cell design; electrode material; reaction environment; three-dimensional electrode.

Contents ***(intended to aid review)***

(Approx. 13,200 words, 1 table, 15 figures, 51 reactions/equations and 113 refs).

Nomenclature

Symbol	*Meaning, Units*
a	Area factor in equation (45), Dimensionless
A	Electrode area, cm^2
A_e	Volumetric electrode area, cm^{-1}
A_{end}	End (flat ring) area of a single cathode or anode component, cm^2
A_i	Volumetric gas-liquid interfacial area, cm^{-1}
A_1	Area of a single electrode element, cm^2
A_{side}	Side (cylindrical) area of a single cathode or anode component, cm^2
A_x	Internal cross-sectional area of tower , cm^2
c	Concentration of tracer in the fluid, mol dm^{-3}
$c_{(0)}$	Initial concentration of metal ion in the reservoir, mol dm^{-3}
$c_{(in)}$	Concentration of metal ion at reactor inlet, mol dm^{-3}
$c_{(out)}$	Concentration of metal ion at reactor outlet, mol dm^{-3}
$c_{(t)}$	Concentration of metal ion in the reservoir at time t, mol dm^{-3}
c_b	Bulk concentration of metal ions, mol dm^{-3}
$\overline{D}$	Dispersion coefficient , $cm^2\ s^{-1}$
E	Electrode potential, V
E_e	Equilibrium electrode potential, V
$E_{e,a}$	Equilibrium electrode potential of anodic reaction, V
$E_{e,c}$	Equilibrium electrode potential of cathodic reaction, V
E_S	Specific energy consumption, kW h kg^{-1}
E_V	Volumetric energy consumption, kW h m^{-3}
F	Faraday constant (= 96 485 C mol^{-1}), C mol^{-1}
h	Electrolyte film thickness down an electrode , cm
I	Current, A
I_L	Limiting current, A
I_T	Total current per unit length of wetted perimeter, A cm^{-1}
j	Current density, A cm^{-2}
j_L	Limiting current density, A cm^{-2}
j_L'	Limiting current density at the end of a bipolar electrode, A cm^{-2}

k_m	Averaged mass transport coefficient, cm s^{-1}
L	Length of the experimental section of the tower, cm
L_m	Length of a single, bipolar electrode, cm
L_{hl}	Half-length of a single, bipolar electrode, cm
L_w	Wetted perimeter per layer of packing, cm
n	Amount of material, mol
$n_{(0)}$	Initial amount of material, mol
$n_{(t)}$	Amount of material at time t, mol
N	Number of bipolar electrode layers in the reactor tower, Dimensionless
N_{layer}	Number of identical components in each electrode layer, Dimensionless
Q	Volumetric flow rate of electrolyte, cm^3 s^{-1}
r_o	Outer radius of a cylindrical Raschig ring, cm
r_i	Inner radius of a cylindrical Raschig ring, cm
s_n	Normalised space velocity, cm^3 cm^{-3} s^{-1}
t	Batch electrolysis time, s
U	Cell potential difference, V
U_e	Cell potential difference at equilibrium, V
U_{stack}	Potential difference over a stack of electrodes in the tower packing, V
v	Mean linear electrolyte velocity, cm s^{-1}
V	Volume of electrolyte in the reservoir in a batch system, cm^3
V_e	Volume occupied by electrode, cm^3
V_n	Electrolyte volume for the normalized space velocity, cm^3
V_R	Effective electrolyte volume in the reactor, cm^3
w	Velocity exponent in equation (17), Dimensionless
x	Distance from the reactor entrance down the tower, cm
$X_{A,s}$	Fractional conversion in a single-pass PFR, Dimensionless
$X_{A,b}$	Fractional conversion in a batch recirculation PFR, Dimensionless
Y_{ST}	Space time yield of the reactor, mol m^{-3} s^{-1}
z	Electron stoichiometry in the primary reaction, Dimensionless

Dimensionless groups

Bo	Bodenstein number, Dimensionless
Pe	Peclet number, Dimensionless
$(Re)_f$	Electrolyte film Reynolds number, Dimensionless

Greek

β	Fractional contribution of electrode ends to the current, Dimensionless
ε	Volumetric porosity of electrode packing, Dimensionless
η	Overpotential (= $E - E_e$), V
$\eta_{a,act}$	Overpotential at anode due to charge transfer, V
$\eta_{a,conc}$	Concentration overpotential at anode, V
$\eta_{c,act}$	Overpotential at cathode due to charge transfer, V
$\eta_{c,conc}$	Concentration overpotential at cathode, V
η_T	Overpotential for one half of a bipolar Raschig ring, V
θ	Dimensionless time (vt/L), Dimensionless
θ_L	Fraction of layer side area which is electrochemically active, Dimensionless
ν	Kinematic viscosity of the electrolyte, $cm^2\ s^{-1}$
ρ	Electrolyte resistivity, ohm cm
τ_R	Mean residence time in the reactor = V_R/Q, s
τ_T	Mean residence time in the reservoir = V/Q, s
ϕ_m	Potential of the solid electrode phase, V
ϕ_R	Equilibrium potential of the anodic reaction with respect to the counter electrode reaction, V
ϕ_s	Potential of the solution liquid phase, V
ϕ_T	Potential across a bipolar electrode with respect to the counter electrode reaction, V
Φ	Overall current efficiency for metal ion removal, Dimensionless

Abbreviations

AOP	Advanced oxidation process
BDD	Boron doped diamond
BTTR	Bipolar trickle tower reactor

CVD	Chemical vapour deposition
PFR	Plug flow reactor
OER	Oxygen evolution reaction
RTD	Residence time distribution
RVC	Reticulated vitreous carbon
3D	Three dimensional

Introduction

The bipolar trickle tower reactor (BTTR), shown in Figure 1, is an example of a columnar, thin film electrolyte reactor using bipolar, porous, 3-dimensional electrodes. These components are arranged in the parallel plane configuration common in electrochemical reactors;[1] in contrast to most cells, the electrode layers and separators are stacked as horizontal layers. Following its introduction in a 1971 patent,[2] the BTTR has developed via an appreciation of its reaction environment, modification of the electrode geometry and a diversification in its applications. The BTTR can be considered as an electrochemical version of an adsorption tower. In its simplest form, its construction is column-based, utilising a high voltage with low current and having a thin film of electrolyte under gravity flow, percolating down the column at a typical mean linear velocity of 0.1 to 10 cm s^{-1}. In contrast, the packed-bed electrochemical reactor is usually deployed with an upward flow of electrolyte and total flooding of the porous electrodes. The BTTR is well suited to replaceable electrode cartridges in environmental treatment.[3] Experience has shown that up to $N = 80$ bipolar electrode layers, hence $N + 1 = 81$ cells, in one column are possible using common (<200 V DC) power supplies.[4] Columns can, however, be as short as <10 layers, with a cell potential difference of <3 V per layer. Early work was largely based on individual Raschig rings (usually hollow carbon cylinders) close packed in a horizontal layer. Such electrode components are tedious to arrange in single or stacked, multiple layers and have limited area, stability and repeatability. Modern BTTR designs should utilise thinner one piece porous, 3D electrode materials, as indicated in later sections.

The BTTR reactor concept

History

As outlined in Figure 2, the BTTR has developed over 50 years. Throughout the 1970s, many reactor geometries were considered for processing of liquids past a solid surface in chemical engineering.[5] Examples include the absorption tower and the sieve plate column.[6] In the late 1970s, a diverse range of electrochemical reactors emerged as practitioners drew analogy with chemical and physical reactor counterparts.[7,8] By the 1980s, a diverse array of electrochemical reactor designs had been introduced.[9-12] In the same decade,

alternative constructions of the BTTR were explored to enable industrial prototypes.[3,13] Their features, performance and typical scale of operation were documented in detail during the 1990s,[14,15] reviews providing a perspective have been found in the 2000s,[16,17] along applications in dyestuffs oxidation for environmental remediation,[18] as well as a recent review of flow reactors for electrochemical technology has appeared.[19] The last decade has seen many and widening opportunities for high-surface-area electrode structures and finishes,[20] along modern surface catalysts, such as boron-doped diamond, BDD.[21] The emergence of additive manufacturing techniques for electrochemical flow reactors[22-24] has provided new opportunities for the fabrication of reactor components, including electrodes, separators and electrically insulating tower encapsulation. The BTTR is well-suited to scaled-up electrochemical operations at high temperatures and pressures,[25] and could increase their energy efficiency and decrease the cost of some electrochemical processes. The further implementation of electrochemical operations in various fields is considered to be important along the path towards sustainable chemical processing.[26]

Features of the BTTR

According to an electrochemical cell classification, the BTTR is considered as an undivided, thin film reactor with static porous 3D electrodes incorporating a bipolar stack of cells.[10-12,17,19] This configuration provides important benefits:

a) a thin electrolyte film promotes good gas disengagement and lowers ohmic drop,

b) porous, 3D electrodes provide a reasonably high volumetric electrode area, aid gas disengagement and allow uniform electrolyte flow, which can be approximated to a plug flow model,

c) bipolar electrical connections to the electrodes preclude the need for direct contact to individual electrodes and layers,

d) a unique fluid contacting pattern is present; electrolyte experiences alternate anodic and cathodic electrode regions, with time, on passing down the tower,

e) a robust and simple design together with a relative ease of construction and sealing; may confer a low-cost alternative to other designs,

f) a low electrolyte pressure drop due to the high volumetric porosity of the electrode stacking,

g) a relatively efficient reactor for processing solutions or wastewaters with low conductivity,

h) the possibility of performing three-phase electrode reactions.

As shown in Figure 1, the key design features of the BTTR include:

a) liquid electrolyte is introduced as a spray, at the top of a vertical column,

b) an inert, porous feeder anode is usually placed at the top of the tower, under the electrolyte inlet with a similar material as a cathode feeder near the bottom of the column,

c) a thin film of electrolyte trickles down the tower under gravity, passing mutually insulated electrode layers, which are identical and arranged horizontally,

d) the overall directions of electrical current and electrolyte fluid flow are parallel,

e) each electrode layer is physically spaced and electrically insulated from its neighbouring layer by a porous polymer mesh,

f) an individual electrode layer can be fabricated from a porous, conductive ceramic (typically carbon) or metal,

g) each electrode layer is bipolar, the lower side (facing the cathode feeder) being positive and the upper side (facing the anode feeder) being negative,

h) electrolyte exits from the bottom of the tower then falls into a holding tank,

i) the batch recirculation mode of operation is commonly used, a fixed volume of electrolyte, V being recirculated,

j) the BTTR utilises a series of undivided cells, use of a membrane or ionic separator presenting considerable difficulties in construction,

k) one-piece container fabrication with no moving parts and simple, stationary, low cost electrodes, in contrast to hydrocyclone or rotating cylinder electrochemical reactors.

Related reactor geometries

The BTTR can also be viewed as being related to several reactor geometries, some of which are presented in Figure 3:

a) a thin film electrolyte cell with a small (<1 mm) gap between monopolar electrodes,[42]

b) a flow-by, thin film electrolyte bipolar interdigitated array, e.g.,[43]

c) bipolar stacked disc, capillary radial outflow (Beck) cell,[44]

d) a bipolar packed bed of carbon particles for nitrate ion removal from waters.[45]

The first three cases are similar in view of the thin film of electrolyte achieved in the vicinity of the electrodes due to a narrow inter-electrode separation and their undivided (membrane-less) form. The fourth case is an example of the flooded packed bed reactor in which the layered porous electrodes are substituted by bipolar particles surrounded by insulator particles.

The BTTR has a similar physical arrangement to a bipolar packed bed electrochemical reactor. It is important to realise that the main difference between them is the direction and nature of the flow. In the BTTR, see Figure 1, the electrolyte flow is introduced at the top and trickles down the electrodes as a thin film, under gravity; in the flooded packed bed reactor, the electrolyte enters at the bottom and is pumped upwards. Several publications presenting packed bed reactors using conductive Raschig rings for degradation of textile dyes could be considered BTTRs after minor modifications.[21,38,46-48]

Another alternative is the bipolar trickle-bed electrochemical reactor, first developed by Oloman et al.[49] In this case, the electrical current and the overall electrolyte flow direction are perpendicular. The porous electrodes are arranged at the sides of impermeable bipolar plates as in a filter-press stack. Although using downwards gravity flow, this design permits the use of membranes or other microporous separators. This reactor has been studied for the production of hydrogen peroxide,[49] propylene oxide[50] and sodium dithionite.[51] A slightly modified design was later applied to increase the efficiency of hydrogen peroxide.[52] Current efficiencies of up to 75% and 87% were achieved for hydrogen peroxide and sodium dithionite. The current paths and efficiency in relation to electrolyte conductivity of this alternative design were modelled for single cells by Kusakabe et al.[53,54]

Many workers, perhaps unaware of the pedigree of the BTTR (or bipolar trickle-beds), have studied related electrode geometries and reactor configurations. An example is a flooded electrolyte cell, utilising vertical monopolar mesh electrodes for oxidation of wastewater from an industrial park sewage treatment plant.[55] The concept consisted on a horizontal rectangular channel with flow-across titanium mesh cathodes and PbO_2/Ti anodes with a large separation of 2 cm. At a current density of 5 mA cm^{-2} and an electrolyte mean linear velocity of 0.021 cm s^{-1} the current efficiency was 16.6%.

Electrode and reactor construction

Electrode materials and form, together with electrical connections and reactor construction, are important in tailoring the BTTR to a particular application, ensuring a versatile design or enabling adequate scale-up and processing in industry.

Electrode materials

There is a major choice in the type of electrode packing for a BTTR layer between a) numerous particles and b) a one-piece material. Particles can take many shapes and degrees of regularity, ranging from monosized,

spheroidal, submillimetre solid particles to larger pellets and hollow, cylindrical Raschig rings. The former may be dispensed into the tower on a weight basis, while the latter can be very tedious to pack individually. Small particles can create problems if they fall through polymer separator meshes and can restrict porosity, increasing pressure drop, lowering electrical conductivity and creating maldistribution of current. In contrast, a convenient, easily handled packing is a one-piece metal or carbon mesh, foam or open felt. There are clear cost/convenience differences between selecting off-the-shelf electrode materials and those needing tailored machining or coating. On the other hand, forms of material and ordered, horizontal layers of electrodes and separator packing are limited by the need to secure a uniform flow of electrolyte, percolating under gravity down the column.

The early choice of electrode packing materials was influenced by consideration of practice in gas-solid or liquid-solid absorption columns in chemical engineering.[5] Such column packings need to be relatively low cost, of simple geometry and easy to mass produce. Typically, their volumetric porosity is in the range 85–95% to offer a high volumetric surface area with a moderate pressure drop. Developments at Southampton and Newcastle universities in the 1970s were mostly carried out in the research groups of Fleischmann, Jansson et al. with conductive Raschig rings.[31-33,35] Some were hexagonally fluted internally but smooth on their outer surface. While absorption columns normally use random packings, the BTTR needs an ordered arrangement, both within each layer (to encourage good flow distribution) and between neighbouring layers (to promote a uniform potential and current distribution). As shown in Figure 4, in the case of Raschig rings,[30] hexagonal close packing in each layer with vertical alignment of rings was favoured but difficult to achieve by manual packing of tower layers. Contemporary cell designs at Newcastle University also used stacked cylindrical carbon rods.[8] The initial choice of Raschig rings seemed logical but was fraught with problems, due to the need to manually position each packing component in each layer then order the layers in a tower. Indeed, a long, straight, rigid metal wire had to be inserted at the top of the tower and extended to locate each Raschig ring from the bottom layer upwards. Some BTTRs had as many as 80 layers with as many as 60

cylindrical rings per layer, necessitating the tiresome, manual location and ordering of thousands of individual electrode components.

In the 1980s, alternative electrode packing geometries and construction of the BTTR were explored by Walsh and Schiffrin at Southampton, to enable industrial prototypes, particularly for precious metal reclamation.[3] Uses in synthesis and electrochemical processing have been considered but primary applications were in wastewater treatment, including metal ion removal from dilute liquors, oxidation of unwanted organics and water disinfection via *in-situ* generation of oxidants.[14,15] Diverse electrode materials, and forms for BTTRs were explored in Schiffrin's research group at Southampton University,[4] responding to the need to improve construction, scale-up and maintenance to realise industrial prototypes. At the time, Walsh et al. prototyped carbonised fluted cardboard and fibreboard which had been impregnated with a phenolformaldehyde resin to provide semidisposable, lightweight and low-cost electrode materials.[4] Carbon forms included layers of packed beds containing numerous particles, crushed activated carbon, rectangular solid rods, mesh, cloth, foam and perforated plate.[3,4] Staggered perforated graphite plates were considered by Sudoh et al.[56] and Franke et al.,[57] while and ferrite pellets were used by Kusakabe et al.[58] Carbon materials for these applications have been compared in Table 1. An indication of diverse electrode forms which have been used in BTTRs is provided in Figure 5. Undoubtedly, one-piece porous, 3D electrode materials for each layer are superior to individual particulate packing components regarding ease of handling, convenience in use and electrical conductivity.

Over the last decade, examples of the use of Magnéli phase titanium oxide electrodes have increased,[59,60] while the popularity of boron doped diamond coatings has encouraged their use as coatings on titanium supports.[61] Unfortunately, such coatings have often been applied to BTTRs on outdated Raschig ring supports,[38,46-48] rather than a more progressive, monolithic electrode supports, such as titanium felt,[62,63] foam,[64] or micromesh[65,66] as well as stainless steel equivalents.[67,68] Felt substrates can be produced by the melt spun process or by sintering metal fibres, foams by powder sintering or coating carbonized polymer foams, and

meshes by expanding sheets or by weaving wires.[20] Moreover, porous electrodes can be made by 3D printing[24,69,70] then coated by electrodeposition.[24,71] The availability of coarse graphite felt[72] and reticulated vitreous carbon (RVC)[73-75] widens the choice of monolithic porous electrode supports.

Electrical connections and feeder electrodes

The electrical, monopolar current feeders of the BTTR are used as terminal connections to introduce and receive current from the electrode packing. It is important they are mechanically robust, do not impede electrolyte flow and are sufficiently corrosion and erosion resistant. In older reactor designs, 6-8 mm thick, perforated carbon plates of were common, although the grade of carbon is important and anodic oxidation leads to some degradation. Oxygen evolution is a common side reaction at anodic feeders and the gas tends to erode the surface as well as oxygenate the electrolyte. Operating the top feeder as an anode comes from the practice of electrodeposition on cathodes in some applications, as shown below; gravity helps keep the cathodically deposited metal under cathodic protection on upward facing parts of the packing.

Early BTTRs commonly used perforated graphite plate electrical feeders,[32] although carbon cloth[31] and Pt wire coils[76] were occasionally used. Later and alternative designs often used coated metal meshes, including stainless steel or platinised titanium.[50] It is particularly important that copper wire connections to the feeder do not contact the electrolyte, to avoid anodic dissolution of metal, damage to the feeder connection and copper dissolution into the electrolyte as ions. Perforated metal plates, gauzes and meshes provide an alternative feeder material but, again, corrosion must be considered, along with the possibility of surface passivation leading to inactivity or ohmic contacts. Titanium mesh (of 1-2 mm thickness) has commonly been used but the metal can corrode in cathode regions via hydride formation,[77] especially in acid electrolytes or else passivate in anode or open-circuit regions due to formation of poorly conductive surface oxide films. Platinised titanium or DSA coated titanium is often a solution to these problems and can survive several years of operation.[78] Occasionally, conductive, non-stoichiometric titanium oxide phases such as Magnéli phases, e.g.

Ebonex®,[59,60] have been used. The recent advent of 3D printing electrode materials has widened the form, size and material choice for carbon-,[69] stainless steel-[24] and titanium-based[71] current feeders.

An improved design of BTTR has been described.[3,4] It involves features such as a) a central electrode feeder, b) replaceable electrode cartridges, c) low cost, single piece, perforated electrode layers and d) a modified electrolyte inlet dispersion. A central electrical connection diminishes the number of cells and the distance between the negative and positive feeders by a factor of two. Access to both feeders is important for inspection, maintenance and replacement. The BTTR design should not entrap a feeder in the tower or result in undue mechanical load being placed on top of a lower feeder, due to the weight of electrode packing. Where possible, separate flanges can facilitate access to the electrical feeders without disturbing other BTTR components during inspection and maintenance procedures.

The high voltage-low current nature of the BTTR must be borne in mind from a safety point of view. The electrical connections should be fully insulated to prevent human contact, due to the possible electrical shock hazard. In adverse circumstances, the bipolar electrode packing may become through conducting, e.g. due to excessive metal or metal oxide deposition. The terminal feeders can then experience the full applied dc potential difference applied (perhaps >200 V) and it is prudent to incorporate current-limiting circuitry, especially in the case of very conductive electrolytes and wide bore external flow tubing.

In the presence of halide ions in the electrolyte,[34,57] the possibility of chlorine or bromine evolution at the anodic feeder must be considered. At high current density, ozone evolution is a possibility in certain acid electrolytes.[79] As in all undivided cells involving aqueous electrolytes, appropriate precautions must be taken to handle off-gases containing hydrogen-oxygen (or in some cases hydrogen-chlorine) mixtures and to select anode surfaces which are not rapidly degraded via corrosive species in the electrolyte, including halide ions.

Reactor construction

The diverse scale of BTTRs constructed by one of the authors has ranged from printed mesh electrode/insulator packings in 'microflow' circular glass tubes, <1 cm in diameter through circular glass columns in pilot scale chemical engineering laboratories of universities through to 5 m diameter plastic drums in industry. Classical designs of BTTR tended to use discrete electrode and insulator components stacked vertically, in an ordered manner, in a circular cross section glass tube, often QVF process glassware on a pilot scale.[37] Such a construction has the advantage of using standard glass tube, metal clamped glass flanges and elastomeric sealing components. In the case of large industrial process installations, several circular or rectangular tower columns may be mounted vertically into an outer polymer tank with the interior partitioned to suit. Each internal tower can be equipped with its own spray inlet, a common exit gulley being provided at the bottom of the outer vessel.

It is important to maintain adequate fluid breaks in the BTTR flow system, including the inlet spray and outlet drain sections, to prevent undue external and internal leakage currents. Flooding of the tower packing, and at the outlet from the tower, must be avoided by venting, such that the tower 'breathes' well and adequate drainage takes place. In the reservoir, feed and return pipes should be located sufficiently far apart to promote not only good mixing but also to prevent excessive externally circulating leakage currents. It is good practice to incorporate a current limiter in the external flow circuit to detect and respond to excessive leakage currents under fault conditions.

3D printing could also applied to the bodies of electrochemical reactors.[23,70] Since it is difficult to justify the use of this technology to manufacture tubes, the aim should be instead to create fully integrated BTTRs, such as already exemplified for filter-press cells,[80] perhaps taking advantage of multi-material 3D printing.[81]

Reaction environment

Adequate design, construction and operation of the BTTR can lead to an impressive performance as long as the reaction environment in the tower is taken into account. In particular, it is important to consider electrolyte flow, current distribution, active electrode area, the rate of mass transfer between electrolyte and electrode and the mode of operation of the reactor. The behaviour of the BTTR can be appreciated by considering the device to show several zones, as indicated in Figure 6:

a) the progress of electrolyte down the reactor involves an entry (inlet and flow conditioning) zone indicated in Figure 6a), the bipolar stack of electrodes separated by plastic meshes in the tower packing, then an outlet zone, facilitating drainage, before the fluid exits the tower.

b) an individual cell is formed between electrode layers, across a thin electrolyte film in the region of the polymer mesh separator as indicated in Figure 6b) and discussed below.

c) an individual layer can be divided into 3 regions as seen in Figure 6c), from the perspective of electrode overpotential. At very negative overpotential at the top edge and down a fraction of the side, a cathode is formed; at the opposite, lower end of the electrode is an anode region; between these regions, in a central part of the porous electrode layer, little or no electrochemical activity is experienced, i.e., the region experiences too low an overpotential to be anodic or cathodic.

d) in the black-box approach of Figure 6d), the BTTR can be viewed as a single pass plug flow reactor (PFR) experiencing a steady volumetric flow rate, Q resulting in a mean linear velocity of electrolyte, v down the tower packing, with the inlet reactant concentration at the top of the reactor, $c_{(in)}$ progressively reaching the outlet concentration, $c_{(out)}$ at the bottom.

Practical considerations are important in design and operation of BTTRs. For example, loss of particulate carbon from the Raschig rings, due to corrosion or erosion, is problematic. These particles tend to block any fine fluid pathways in the spray nozzle at the top of the tower (reactor inlet) causing non-uniform flow dispersion and back pressure. Most studies have used an external reservoir to hold, condition and recirculate the electrolyte via a pumped circuit. Such an arrangement also allows the flow circuit/reservoir loop to assist

heat management, cooling being necessary due to Joule heating in the BTTR. A recent study has utilised a jacketed glass column BTTR, the outer glass cylinder acting as a water cooler.[21]

Fluid flow

The BTTR is a thin film reactor operating under gravity flow of electrolyte. Electrolyte flow is normally steady, providing a continuous, thin film trickling down the column. The range of volumetric flow rate, Q (hence mean linear velocity, v) must be high enough to adequately wet all parts of the electrode packing and achieve a moderately high mass transfer of electroactive species to, or from, the electrode surface. On the other hand, an excessively high electrolyte flow rate involves a higher pressure drop (and pumping cost) across the inlet and packing; high flow may also result in flow bypassing through each layer or past several layers in the tower, leading to inefficiencies in performance. The electrolyte flow rate depends on the geometry of packing and tower. The tower packing must allow free and uniform fluid flow while the outlet is often larger in cross section than the inlet to facilitate 'breathing' of the reactor to enable free flow under gravity. Process intensification in trickle tower reactors can be achieved using pulsatile flows,[82] albeit at increased cost and pumping complexity.

The local electrolyte flow conditions are complex in a BTTR since they are so dependent on the geometry and order of the electrode and separator as well as on the volumetric porosity. The nominal, mean linear flow velocity of electrolyte down the tower, v, past the electrode surface, is the ratio of volumetric flow rate to the averaged cross-sectional area of an electrode area:

$$v = \frac{Q}{\varepsilon A_x} \tag{1}$$

where ε is the volumetric porosity of the electrode packing and A_x is the cross sectional area of a single layer. Ideally, v will be the same throughout the tower packing. This calls for uniform flow distribution, a sufficiently

high volumetric flow rate and a uniform packing of sufficient and uniform porosity. In practice, values of mean linear flow velocity downwards past the electrode surface are typically limited to the low end of the range 0.1-10 cm s^{-1}. The porosity is not only affected by free space due to packing voidage but also by the presence of time dependent off gases from the electrodes. In practice, $0.10 > \varepsilon > 0.60$; close packed Raschig rings typically achieve a value of $0.50 > \varepsilon > 0.60$.[83] In contrast, $\varepsilon < 0.95$ in open-foam metal electrodes.[84] It is unfortunate that few studies in the literature have stated, or shown an awareness of the importance of electrolyte flow velocity to reactor performance.

In order to achieve an adequate radial dispersion of flow over the tower, the inlet is particularly important; two features are critical:

a) an effective electrolyte spray, which may take the form of a simple showerhead (possibly a perforated glass one) or a more sophisticated spray nozzle having a suitable filled circular or rectangular flow cone to match the internal tower geometry.

b) an inlet flow dispersion zone, typically consisting of a porous, e.g., dummy electrode material, such as ceramic Raschig rings in early designs or perforated polymer meshes.

As a black-box, the BTTR can be simply modelled as a PFR, non-ideal flow occurring due to axial dispersion. Concentration-time behaviour of a tracer in the exit stream of the vessel can be used to establish the degree of dispersion via stimulus-response techniques.[85] The tracer has been typically a conductive salt[86] or a dye.[87] The environment in porous in BTTRs has been described from experimental measurements using an electrochemical tracer.[28] In this alternative technique, a cupric ion concentration pulse was injected near the inlet of the reactor then the cupric ion mixing history was followed at the outlet by cathodic deposition of copper under limiting current conditions. The data could be rationalised against lumped parameter models using dimensionless groups, enabling residence time distribution curves to describe the hydrodynamics according to a dispersed PFR model.

A dimensionless Peclet number, *Pe*, can be used to generalise flow dispersion within the PFR reactor.[88] It is defined as:

$$Pe = \frac{vL}{\overline{D}} \quad (2)$$

where ν, L and $\overline{D}$ are the mean linear velocity of the electrolyte past the electrode surface, the length of the experimental section of the reactor and dispersion coefficient, respectively.

The axially-dispersed PFR model incorporates the Peclet number and gives a good approximation of the experimental observations by assuming that dispersion takes place only in the direction of fluid flow.[37] It is described by the equation:

$$\frac{\partial c}{\partial \theta} = \left[\frac{\overline{D}}{vL}\frac{\partial^2 c}{\partial x^2}\right] - \frac{\partial c}{\partial x} \quad (3)$$

where c is the concentration of tracer, θ is the dimensionless time and x is the distance from the reactor entrance down the tower. On the basis this model and Cu^{2+} ion tracer residence time distribution (RTD) measurements, it has been shown that the flow in a BTTR can be considered to comprise of a fast and a slow moving phase with dispersion in the fast phase down the packing material, a degree of exchange between the phases.[89]

Likewise, a mass balance for the reactant concentration in the axial direction of the dispersed PFR reactor containing 3D electrodes can be written as:[90]

$$\frac{\partial c}{\partial t} = \overline{D}\frac{\partial^2 c}{\partial x^2} - v\frac{\partial c}{dx} - \frac{\partial n}{\partial t}x \quad (4)$$

where the dispersion coefficient, $\overline{D}$ describes a degree of turbulent mixing superimposed on the ideal plug flow.

The steady state polarisation behaviour in a BTTR under complete mass transfer controlled conditions was studied for $Fe(CN)_6^{3-}$ reduction on carbon,[31] showing that overall behaviour, in the axial direction down the tower, could be described via a one-dimensional, lumped parameter model according to the expression:

$$\frac{h}{\rho}\frac{\partial^2 \phi_s}{\partial x^2} = -\frac{h}{\rho}\frac{\partial^2 \eta}{\partial x^2} = -zF\frac{\partial n}{\partial t} \quad (5)$$

where h is the electrolyte film thickness, ρ is the electrolyte resistivity, ϕ_s is the potential in the solution phase, η is the overpotential at the electrode and n is the amount of reactant transformed in a z electron reaction in time t. However, the products of reaction can be mixing sensitive and it is desirable to describe the flow conditions inside the reactor, including the degree of dispersion.

The figures of merit derived from the mean residence time, such as the space-time or space-velocity, must be calculated by considering the existence of stagnant regions and other non-idealities established in tracer experiments. The film Reynolds number, which characterises fluid flow down the Raschig rings, can be defined as:[31]

$$(Re)_f = \frac{Q}{2\pi N_{layer}(r_0 + r_i)\nu} \quad (6)$$

which assumes that the electrolyte film thickness along the wetted perimeter of the Raschig ring is equal to the film thickness along the inner wetted perimeter. Expressions for film Reynolds number should be developed for the case of other porous electrode layers, such as metal mesh or RVC.

Mean residence time values from the first moment of the curves obtained from tracer experiments have been calculated as a function of the film Reynolds number by Trinidad et al.[37] in the modelling of a Raschig ring based BTTR. See below. The dimensionless Peclet number[89] was used as a simple strategy, based on the first and second moments of the mean residence time curves and *Pe*. The tracer technique led to higher residence time values as it considers tailing effects, rather than the nominal, averaged values of reactor residence time predicted by the calculation of V_R/Q values which presume ideal, plug flow behaviour within the reactor, as shown in Figure 7.

A more detailed consideration of fluid flow in a BTTR with Raschig ring packings has been made by Fleischmann and Ibrisagić.[89] A circular glass column with closely packed carbon Raschig rings was used to develop theoretical expressions and pursue experimental measurements. The dimensionless Bodenstein number is defined as:

$$Bo = Pe\frac{L_m}{L} \qquad (7)$$

where L_m is the length of the electrode layer (e.g., the height of a Raschig ring) and L is the overall length of the reactor. *Bo* represents mixing over the length of a single Raschig ring. *Bo* values of 0.23 and 0.33 were found by Trinidad et al.,[37] which are similar to values reported by Fleischmann and Ibrisagić[89] for a reactor volume approximately four times smaller. Despite the differences in the reactor geometry between references

[37] and [89], there was no effect of reactor length when Bodenstein numbers were compared. On the other hand, the Peclet number describes dispersion over the reactor, revealing differences between the two sets of reactors.

Modern numerical methods involving the simulation of hydrodynamics within the trickle flow in BTTRs have not been developed yet. However, the possibility of modelling trickle flow has been shown by Souadnia et al. for the case of trickle bed reactors.[91] Their one-dimensional approach focused on establishing the boundary conditions for a non-electrochemical two-phase system and the prediction of liquid saturation and pressure drop. Notably, an electrochemical technique was employed to quantify the mass transfer characteristics of the same reactor.[92] An analogous modelling approach could be developed for layered, porous materials in BTTRs by neglecting the gas flow and saturation and considering the electrolyte film velocity and porosity at the bipolar electrodes.

Current distribution and bypass (leakage) current

The first comprehensive measurements of current and potential distribution on BTTRs packed with carbon Raschig rings separated by monofilament, 1 mm thick polyester mesh, were described by Fleischmann and Ibrisagić.[31] The tower comprised a 4 cm internal diameter glass column containing 14 layers (hence 15 cells, including the electrical feeders); each layer contained 30 Raschig rings, each of 0.63 cm external diameter. Local axial and radial currents in selected layers were monitored using split Raschig rings and an external current follower; the potential of each layer was measured with respect to the lower current feeder. The electrode potential is due to the difference between the potentials of the solid electrode phase, ϕ_m and solution phase, ϕ_s:

$$E = \phi_m - \phi_s \tag{8}$$

For simplicity, the electrode phase can be considered to be equipotential and changes in electrode potential arise due to local differences in the solution potential down the tower. A charge balance over an electrode layer can then be written as:

$$\left(\frac{d\eta}{dx}\right)_{x=L_{lh}} = \left(\frac{d\eta}{dx}\right)_{x=-L_{lh}} = I_T \frac{\rho}{h} \qquad (9)$$

where I_T is the current per unit length of the Raschig ring perimeter, h is the electrolyte film thickness and ρ is the electrolyte resistivity. If the overpotential at the electrode, η is taken as zero in the centre, i.e., $\eta = 0$ at $x = 0$, modelling of the potential distribution down a distance in the axial direction, x along a single bipolar cylindrical electrode then takes the hyperbolic sine shape indicated in Figure 6c).

In further studies,[89] a plot of potential as a function of layer number was linear through the origin, showing the axial distribution of potential to be uniform, i.e., the stack potential being equally divided over the number of cells at the film Reynolds number involved $Re_f = 18.6$. During the measurements, a 0.01 mol dm^{-3} H_2SO_4 solution containing equimolar concentrations (0.001-0.005 mol dm^{-3}) $Fe(CN)_6^{4-}$ and $Fe(CN)_6^{3-}$ ions was circulated a through the BTTR. The radial potential distribution showed a higher potential outwards from the centre of a layer, the difference in potential being most marked for a Raschig ring near the centre of the layer experiencing a high liquid flow rate. Such a radial non-uniformity of potential can be readily overcome using a one-piece electrode layer and improved electrolyte distribution.[4]

Early measurements involving complete mass transfer control of redox reactions on Raschig rings[31] also showed the film thickness of electrolyte down the electrode surface, h to increase with flow rate, according to:

$$\eta_T = \frac{\rho}{h} I_T L_{hl} - \frac{\rho}{4h} j_L {L_{hl}}^2 - \beta \frac{j_L{}'(r_o - r_i)\rho L_{hl}}{2h} \quad (10)$$

where β is the fractional contribution from the electrode ends and ρ is the electrolyte resistivity. The electrolyte film thickness, h increased from 0.031 to 0.049 cm and the limiting current density for $Fe(CN)_6^{3-}$ reduction, j_L increased by 135% from 0.40 to 0.54 mA cm^{-2} as the volumetric flow rate of electrolyte was increased from 600 to 1400 cm^3 min^{-1}, corresponding to $(Re)_f$ = 11.1 to 26.0.

Such early studies indicated a reasonable axial potential distribution and indicated that a fraction of the side of the ring area, θ_L was active. Studies attempting to quantify θ_L and relate it to electrode geometry and process conditions awaited studies by Jansson et al.,[32,33,35] as described below.

The flow of leakage (stray or bypass) current is a problem in all bipolar electrode reactors.[13,17] In the BTTR,[57,58] a fraction of the total current in a stack, instead of passing in series through the electrode layers, flows a) internally through the electrolyte within the porous layers, b) past the layers or c) through the external flow circuit around the reservoir, pump, inlet and outlet. In BTTRs, leakage currents can be minimised by using a low conductivity electrolyte,[58] maintaining a thin electrolyte film on the electrode surface and breaking the external flow loop in places, e.g., with a liquid-air gap. Including ones between the shower inlet and the top of the tower packing and the drainage area near the outlet at the bottom of the tower. Clearly, there are compromises to be made in the interests of achieving a good BTTR performance. Typically, leakage currents can be minimised to <2% of the total current.

Studies of diverse packings in a BTTR by Walsh et al.[3,4] measured external, pumped electrolyte circuit, leakage currents in 2- and 3-feeder designs having similar overall electrode areas. These detailed studies of several BTTR geometries culminated in the recommendation of a 3-feeder system, incorporating a central

back to back anode and electrically joined and grounded feeders at the top and bottom of the tower packing. Such an arrangement, shown in Figure 8a), led to minimal external leakage currents in the electrolyte-tank flow circuit and safe operation.

More recently, Perez and Bisang have provided a treatment of theoretical and experimental aspects of electrochemical reactors with bipolar 3D, porous electrodes via a mathematical model.[39] Their work calculates leakage currents under mass transfer control at low overpotentials and was validated by measuring the mass of anodically dissolved and cathodically deposited copper from a stack of copper meshes used as a porous electrode ($\varepsilon = 0.70$). The electrical current passing through the electrodes in the flooded, rectangular channel cell is perpendicular to the electrolyte fluid flow, as shown in Figure 9a). By considering the geometry of the electrode, the resistivity of the electrolyte and the kinetic parameters, it was found that although the primary current distribution was homogeneous, the axial current distribution was significant due to ohmic drop in the electrolyte and polarization; the leakage current decreased as the total current was augmented, as shown in Figure 9b). A modified version of the model, considering downward trickle flow of a film of electrolyte with current flow in the same direction could be developed to describe porous electrodes in BTTR operation.

Electrode potential distribution and active electrode area

One of the most important electrode characteristics governing BTTR performance is the volumetric electrode area of the packing, i.e., the ratio of active electrode area to the space occupied by the electrodes:

$$A_e = \frac{A}{V_e} = \frac{NN_{layer}A_l}{A_x L} \tag{11}$$

The electrode area, A is particularly important in the BTTR. It is not always easy to measure geometrically, due to the possibility of using complex shapes of porous, 3D packing materials and may change with time, reaction environment and operational conditions more than in most electrochemical reactors.

In the case of hollow cylindrical electrode elements, the top and bottom 'end areas', the end area of a single cathode or anode A_{end} may be expressed as that of flat, concentric rings, i.e.:

$$A_{end} = \pi(r_o + r_i)^2 \tag{12}$$

Due to the potential distribution down a bipolar electrode layer, a fraction, θ_L of the external and internal cylindrical walls of cylindrical Raschig rings is also active, due to the potential distribution, the side active area being:

$$A_{side} = 2\pi\theta_L(r_o + r_i) \tag{13}$$

The end (top and bottom) plus side active area of a cathode or anode zone can be summed to give the total area of a single anode or cathode zone as:

$$A = A_{end} + A_{side} \tag{14}$$

Laboratory studies of metal ion removal and cyanide oxidation by Jansson et al.[33,35] in two Raschig ring packed models of BTTR found the side active area, averaged over batch recirculation trials, to be in the range 0.11 to 0.34. The value of θ is complex and depends on interaction with electrolyte composition, time, electrode potential, reactant concentration and electrolyte conductivity. The deposition of conductive metal in cathode zones can result in a θ_L value which is not only time-dependent but also modifies the potential distribution down a layer. In a conservative approach to BTTR design and selection, electrode area can be solely based on

the end area of an electrode layer. The additional area arising from the side active area can be viewed as a bonus.

A simple expression for the total electrode area in a BTTR may be the product of number of identical layers, number of electrode components in each layer and the end area of each electrode:

$$A = NN_{layer}A_{end} \tag{15}$$

Mass transfer

As explained above, current bypass is minimized in BTTRs by utilizing dilute reactant concentrations and a thin film of electrolyte. Under such conditions, the electrode reaction typically falls under mass transport control. This implies that the limiting current established by the convective-diffusion rate of reactant to the electrode surface, I_L sets the maximum rate of conversion. If these conditions are met over the entire electrode surface, the steady state limiting current is given by the expression:[13]

$$I_L = zFc_b k_m A_e V_e = zFc_b k_m A \tag{16}$$

where c_b is the concentration of electroactive species, k_m is the mass transport coefficient, A_e is the volumetric electrode area and V_e is the electrode volume.

The product $k_m A_e$ can be considered as a performance factor for 3D, porous electrodes and may be used in comparisons and scale-up. It can be readily appreciated that electrode materials with a high volumetric surface area and effective mass transport features are beneficial to the operation of a BTTR. Interestingly, given the heterogenous nature of the reactions, an analogue of $k_m A_e$ is found as a in conventional (non-electrochemical) trickle towers as the performance factor $k_m A_i$, where A_i is the volumetric gas-liquid interfacial area.[5]

In a simplified, but practical approach, the limiting current is related to the mean linear velocity of electrolyte past the electrode surface by an empirical power law:[17]

$$I_L = Kv^w \tag{17}$$

The constants K and w depend on the electrode geometry, electrolyte composition, solution transport properties and temperature.

The role of the products k_mA_e or k_mA in the description of the factional conversion of reactant over time is explained below. However, it can already be appreciated that the active electrode surface area is essential to the description of the limiting current; see equation (16). Yet, only a fraction of the electrode layer geometrical surface area can be considered an electrochemically active area. The value of this fraction, θ_L is difficult to predict as it depends on electrolyte shape and composition, the type of electrode reactions and the potential distribution. El Ghaoui and Jansson electrolysed copper, nickel and zinc cyano complex electrolytes to deposit metal at cathode zones and oxidise cyanide at anodic zones under mass transport control.[35] They expressed the reactant conversion of the electrolyte in the tank through equation (28) in terms of θ_L:

$$\ln\left[\frac{c_{(t)}}{c_{(0)}}\right] = -\frac{t}{\tau_T}\left[1 - \exp\left(\frac{k_m\theta_L L_m L_w N}{Q}\right)\right] \tag{18}$$

where the symbol L_m is the length of a bipolar electrode, L_w is the wetted perimeter per layer, N is the number of layers and τ_T is the residence time in the tank.[35] The dimensionless term t/τ_T is the number of recycles of electrolyte through the tank. The experimental data was analysed via a semilogarithmic plot of *c(t) vs. t*, allowing the fraction of side active area, θ_L to be estimated. Values in the range of 0.11 to 0.48 were generally found and θ_L is approximately given by the expression:[33,35]

$$\theta_L = 1 - \frac{\phi_R}{\phi_T} \quad (19)$$

where ϕ_T is the potential difference across one electrode layer and ϕ_R is the equilibrium potential of the anodic reaction with respect to the counter electrode reaction.

Mode of operation

Batch recirculation of a fixed volume of electrolyte in a reservoir downwards through a BTTR, using a magnetically coupled centrifugal pump, is the most common mode of operation. Such an operation allows flexibility in choosing electrolyte volume and composition, facilitates sampling of the electrolyte, pH and temperature control. Under complete mass transport controlled conditions, the reservoir reactant concentration history can be described by equation (28). The single pass mode of BTTR operation has occasionally been used. In the steady state, under complete mass transport controlled conditions, conversion over the reactor is described by equation (30).

Reactor performance

Overall reaction rate

Important expressions describing the performance of a BTTR include those involving the overall rate of a reaction (allowing for current efficiency), the rate per unit reactor volume, the sources of cell potential difference losses and expressions relating fractional reactant conversion to reactor characteristics and operational conditions.

The current flowing in series through *each* cell of the BTTR can be viewed as the product of current density, volumetric area of electrode and electrode volume:

$$I = jA_eV_e \quad (20)$$

For a given electrode volume, the importance of achieving a high volumetric electrode area in the packing and maintaining a reasonable current density for the desired reaction are obvious.

The overall rate of an electrode reaction can be written in terms of the reaction rate as the amount of reactant removed per unit time:[93]

$$\frac{dn}{dt} = \frac{\Phi IV}{zFV_R} \tag{21}$$

where V is the volume of electrolyte in the reservoir in a batch system, V_R is the effective electrolyte volume in the reactor and Φ is the current efficiency, which allows for a fraction of the current being used in secondary reactions, typically hydrogen and oxygen evolution in cathodic and anodic zones, due to electrolysis of an aqueous electrolyte.

Cell and stack potential difference

When current flows through a BTTR, the cell potential difference, U across each of the N-1 identical cells may be expressed as:[19,41]

$$U = U_e + \sum|\eta| + \sum|IR| \tag{22}$$

The first summation term on the right-hand side represents all the electrode overpotentials and the second summation term represents the contributions of ionic and electrical resistances. U_e is the thermodynamic cell potential difference at the equilibrium, given by the expression:

$$U_e = E_{e,a} - E_{e,c} \tag{23}$$

where $E_{e,a}$ and $E_{e,c}$ are potentials of the anodic and cathodic reactions at the equilibrium.

The summation of overpotentials deserves more attention, as it describes the contribution of charge transfer polarization at the electrodes and the mass transfer. A detailed expression is:

$$\sum|\eta| = |\eta_{c,act}| + |\eta_{a,act}| + |\eta_{c,conc}| + |\eta_{a,conc}| \quad (24)$$

where $\eta_{c,act}$ and $\eta_{a,act}$ are the cathodic and anodic activation overpotentials, respectively, and $\eta_{c,conc}$ and $\eta_{a,conc}$ are the cathodic and anodic concentration polarisations. The first two prevail at low current densities while the latter two at high current densities. The activation overpotentials can be reduced by choosing highly active catalysts and by increasing temperature. Meanwhile, the minimisation of concentration polarisation can be achieved by using large surface area electrode materials or by increasing forced convection, i.e., electrolyte flow rate.

The potential difference across a top and bottom (2- feeder) stack, allowing for the current feeders to provide an additional bipolar layer, is then:

$$U_{stack} = U(N+1) \quad (25)$$

Fractional conversion of reactant

The fractional conversion of reactant over the BTTR at a given time, in terms of the inlet and outlet reactant concentrations:

$$X_{A,S} = 1 - \frac{c_{in}}{c_{out}} \quad (26)$$

and in a recirculating, well-mixed external reservoir:

$$X_{A,b} = 1 - \frac{c_{in,t}}{c_{out,0}} \tag{27}$$

can be related to the operating conditions then used to illustrate factors governing reactor performance, as considered in the following sections.

Batch recirculation mode. A convenient mode of operation is batch recirculation of a fixed volume V_R from a reservoir through the BTTR, which is considered as a PFR. The concentration history in the reservoir involves the decay of an initial reactant concentration, $c_{(0)}$ to a level $c_{(t)}$ at time t, as described by the design equation:

$$\ln\left[\frac{c_{(t)}}{c_{(0)}}\right] = -\frac{t}{\tau_R}\left[1 - \exp\left(\frac{k_m A}{Q}\right)\right] \tag{28}$$

This expression is similar to equation (18) but the mean residence time in the reactor τ_R is used instead of τ_T, showing that the conversion over the reactor can easily be measured and related to reservoir conversion.[37] Both reactor and tank conversion and residence time expressions are important and mutually time-locked. The fractional conversion of reactant per a single pass over the reactor is represented by the term in the square brackets on the right-hand side.

Commonly, the residence time experienced by the electrolyte in the reactor is considerably smaller than that in the tank, i.e. $\tau_R << \tau_T$. Thus, if a simple batch model is implemented considering V as the total volume of electrolyte, equation (28) can be reduced to the form:

$$\ln\left[\frac{c_{(t)}}{c_{(0)}}\right] = -\frac{k_m A}{V} t \qquad (29)$$

Assuming constant values of V and k_mA, the resulting plot of normalised concentration as a function of time should be linear and of slope k_mA/V.[37] In situations where the fractional conversion per pass through the BTTR is small, for instance under high flow rate, this simplified model provides a reasonable description of the reactor operation.[13]

Single pass mode. For convenience and to minimise pumping requirements, a BTTR can be gravity fed from a header tank above the reactor, as long as adequate flow dispersion is achieved within the tower. If a steady volumetric flow rate of electrolyte, Q descends the tower, the inlet concentration, $c_{(IN)}$ exponentially decays down the active length of the tower, L and the terminal concentrations of reactant, over the reactor, can be described by the design equation for a single pass PFR:[37,85]

$$\ln\left[\frac{c_{(in)}}{c_{out}}\right] = -\frac{k_m A}{2.3Q} \qquad (30)$$

where k_m is the averaged mass transfer coefficient and A is the total electrode area of the tower involved in the desired reaction.

Figures of merit

Several figures of merit can be calculated to facilitate a comparison of a) different packings for a given reactor, b) several types or scales of BTTR, c) various process conditions including electrolyte composition or d) different reactors. It is important to apply several of these performance indicators and to consider cost as well as practical, operational factors.

For an electrosynthesis, the amount of reactant consumed, n hence product realised per unit reactor volume, V_R per unit time, t is known as the space time yield, Y_{ST}, which may be expressed by rearranging equation (21) in terms of V_R as:[14]

$$Y_{ST} = \frac{1}{V_R}\frac{dn}{dt} = \frac{\Phi I}{zFV_R} \tag{31}$$

It is important to maximise the current efficiency for the desired reaction and the current by designing a reactor having a suitable electrode area and reaction environment.

In the case of liquid effluent treatment, reactor performance can be quantified by the normalised space velocity,[93] which is the volume of electrolyte treated in a unit volume reactor, in unit time, such that a tenfold change in reactant amount occurs. For a batch system,[13] s_n can be defined as:[94]

$$s_n = \frac{\Phi I}{\Delta nzF}\log\frac{n_{(0)}}{n_{(t)}} \tag{32}$$

In terms of the reactant concentration in a constant volume of electrolyte,[14] this expression may be written:

$$s_n = \frac{\Phi I}{\Delta nzF}\log\frac{c_{(o)}}{c_{(t)}} \tag{33}$$

At constant current, the specific energy consumed in electrolysis, E_S can be expressed as:

$$E_S = \frac{\Phi I U}{V \Delta c} \tag{34}$$

where Δc is the change in reactant concentration of a constant electrolyte volume, V.

During environmental treatment of solutions, it is useful to quantify electrolytic energy use using the normalised volumetric energy consumption, E_V:

$$E_V = \frac{\Phi I U}{V} \tag{35}$$

where V is the unit volume of electrolyte processed.

The volume of solution which can be electrolysed in a unit reactor volume per unit time, such that the reactant concentration is decreased to 10% of its initial value, i.e., with a fractional conversion, $X_A = 0.90$ is also known as the normalised space velocity, s_n:

$$s_n = \frac{V_n}{V_R t_R} \tag{36}$$

where V_n is the electrolyte volume which has undergone a tenfold reduction in reactant concentration and τ_R is the residence time of electrolyte in the reactor. For a single pass PFR, such as the BTTR,

$$s_n = \frac{\Phi I}{zFV_R[c_{in} - c_{(out)}]} \log \frac{c_{(in)}}{c_{(out)}} \quad (37)$$

Such that s_n can be readily calculated from the terminal reactant concentrations in the steady state.

Operational problems

Despite the simplicity of its design concept and operation, the BTTR can experience a number of problems in practice. The following is a summary from 40 years of experience in design, construction and operation of such reactors in the laboratory and in industry:

1. Blockage of the inlet distributor, spoiling the radial distribution of electrolyte flow.

2. Poor electrical contact to the end feeder electrodes, resulting in ohmic losses, heating and electrode degradation.

3. Degradation of bipolar electrodes due to erosion by, or anodic oxidation/open circuit corrosion in, the electrolyte.

4. Difficulty in accessing cell components in the reactor, during assembly, for inspection or to enable replacement.

5. Poor axial flow distribution due to irregular packing of the electrode-insulator layers.

6. Poor current and potential distribution along the tower, due to irregular packing of, or conductivity differences in the electrode-insulator layers.

7. High bypass currents, hence low current efficiency, due to the use of a highly conducting electrolyte, too thick an electrolyte film or a flooded tower packing.

8. Time-dependent performance due, e.g., to corrosion of deposited metal or physical shifting of electrode layers or insulating separators in the column packing.

Unfortunately, some authors have failed to allow for the fact that current passes in series through each bipolar electrode layer in the BTTR.[95] This leads to erroneous calculation of current efficiencies >100% if a Faraday's laws of electrolysis calculation does not acknowledge that the current passes in electrical series through N layers. The overall current efficiency, Φ i.e. the product yield based upon the electrical charge passed during an electrode reaction can be correctly calculated from:

$$\Phi = \frac{\Delta c V z F}{\int N I dt} \tag{38}$$

where N is the number of identical electrode layers which experience the passage of a current, I in the BTTR and V is the total volume of electrolyte.

Applications

The majority of BTTR applications have involved some synthesis of inorganic and organic chemicals, together with removal and recovery of metal ions and complexes and environmental remediation.

Inorganic electrosynthesis

A number of inorganic products have been involved in BTTR synthesis. The first example consists on the electrolysis of sodium bromide, studied by Boussoulengas et al.[27,29] for the epoxidation of alkenes, as shown below. The oxidation of bromide ions at the anode is:

$$2\mathrm{Br}^- - 2e^- \rightleftarrows \mathrm{Br}_2 \tag{39}$$

The reaction was considered in isolation in order to develop a simplified, lumped mathematical model considering the non-uniform reaction rates within a BTTR with up to 67 Raschig ring bipolar layers with 1 mm separators for concentrations between 0.001 and 1.0 mol dm^{-3}.[27,29] Typical space time yields up to 111.8 mol m^{-3} s^{-1} and an energy yield of 2.9 kWh kg^{-1} were achieved for the application. Sudoh et al.[56] then used the same reaction to demonstrate a 50 mm internal diameter BTTR having bipolar electrodes based on staggered, 1 cm thick perforated graphite plates separated by a 5 mm gap. A simple model for current efficiency of bromine generation from a 0.1 mol dm^{-3} sodium bromide was validated and showed that low conductivity decreased energy consumption, and that water electrolysis dominated above 2.7 V unit cell voltage, imposing a limit to the process efficiency. Superficial electrolyte velocities up to 1.2 cm s^{-1} were evaluated. The analogous oxidation of iodide to iodine was carried out during the dehydrodimerisation of diethyl malonate.[76] However, this reaction was studied only as part of the organic electrosynthesis.

Later, Ögütveren et al.[96] studied the regeneration of Co(III) acetate from Co(II) acetate in order to regenerate a spent catalyst used in the production of terephthalic acid from p-xylene by oxidation. The 22 mm internal diameter BTTR was packed with 30 layers of 6 mm diameter, 6 mm long graphite Raschig rings, separated by polyester mesh. The electrolyte was a 0.05 or 0.1 mol dm^{-3} solution of Co(II) in 0.3 mol dm^{-3} sodium acetate in a 90% vol. acetic acid/water mixture. Anodic regeneration of Co(III):

$$\mathrm{Co(II)} - e^{-} \rightleftarrows \mathrm{Co(III)} \qquad (40)$$

was accompanied by oxygen evolution as a side reaction:

$$2H_2O - 4e^- \rightleftarrows O_2 + 4H^+ \quad (41)$$

The cathode reaction was hydrogen evolution in acid media:

$$2H^+ + 2e^- \rightleftarrows H_2 \quad (42)$$

together with some reduction of Co(III) via the reverse of reaction (40). The potential drop per layer was not stated but current density at the end of the electrodes was approx. 20 – 100 mA cm^{-2}. The authors attributed the poor performance to inadequate mixing between layers but it is more likely that the very low mean linear flow velocity used (up to 0.04 cm s^{-1}) gave rise to inadequate mass transport rates. The performance was poor and no better than an undivided planar electrode cell. Space time yields up to 18 kg m^{-3} h^{-1} being achieved with specific energy consumption of 0.5 – 3.5 kW h kg^{-1} at a Co(II) concentration of 0.1 mol dm^{-3}.[96] However, it is worth noting that the study highlighted the variation of space time yield at different mean linear flow rate values as a function of the current row of rings down the tower, as shown in Figure 10a) and Figure 10b), for initial concentrations of 50 mol m^{-3} and 100 mol m^{-3} of Co(II) ions, respectively.

Another example is the regeneration of manganese(III) acetate developed by Güvenç et al.[95,97] for the catalysis of oxidation of aromatic hydrocarbons. The BTTR had 32 layers with an internal diameter of 17 mm and was also operated as a flooded packed bed reactor. Each layer contained 3 Raschig rings with a separation gap of 1 mm. The anodic reaction was:

$$Mn(II) - e^- \rightleftarrows Mn(III) \quad (43)$$

Secondary reactions (41) and (42) took place. For a Co(II) ion concentration of 0.1 mol dm^{-3} and a volumetric flow rate of 0.04 cm^3 s^{-1} (superficial velocity was not given) the maximum space time yield was poor at 22.14 kg m^{-3} h^{-1}. The very low flow rate and the possibility of flow bypass through the small number of Raschig rings per layer might have resulted in non-uniform electrolyte film thickness flow bypass, leading the authors

to conclude that operation as a flooded packed-bed was advantageous. In further work,[97] the same authors optimized the operational conditions of their experimental arrangement in packed bed mode using the 'simplex' algorithm.

Organic electrosynthesis

The first description of an organic electrosynthesis in a BTTR is the hydrodimerisation of acrylonitrile into adiponitrile,[27] following the interest at the time on this reaction.[98] Limited results were shown in order to demonstrate the dependence of the yield of the by-products propionitrile and γ-hydroxy-γ-methylvaleronitrile on the film Reynolds number and the description of a fast- and a slow-moving phase.

Subsequent work by Jansson et al.,[76,99] focused on the effect of reactor design on the productivity and selectivity on convergent paired organic electrosynthesis, in which both anodic and cathodic reactions are utilized to form a desirable product.[100] The production of adiponitrile in the BTTR was reconsidered in order to compare the productivity and selectivity of electrode reactions against a parallel plate flow cell, a capillary gap cell, a pump cell and a stirred tank reactor,[99] all of them having the same electrode surface area of 50 cm^2 for both anodes and cathodes. The chemical step dominated, although the rate of the product and sub-products was affected by the mass transfer. Thus, the BTTR outperformed most designs in terms of conversion except for the pump cell, which is difficult to scale up.

In contrast, the electrosynthesis of 2,5-dihydro-2,5-methoxy-furan showed no dependence on mass transfer in the same study,[99] but instead on the acidity of the reaction layer at the cathodes. In this case, the selectivity of the BTTR was favourable over other reactor designs except for the pump cell. Continuing with the comparison of reactor designs, the same researchers later performed the dehydrodimerisation of diethyl malonate in the BTTR and in the cells mentioned previously.[76] Notably, an organic electrolyte was used, namely acetonitrile saturated with potassium iodide. The cathodic reaction is likely to have involved the reduction of diethyl malonate, while the anodic reaction produced iodine. A chemical step then produced ethyl-1,1,2,2, ethane

tetracarboxylate. It was found that only the pump cell and the BTTR could achieve conversions over 70%, the latter necessitating a lower capital cost.

Later, dedicated studies on the epoxidation of alkenes, including ethylene and propylene, were carried out by workers at Southampton using Raschig rings[29,30,34] and at Dresden using perforated plate electrodes,[57] seeking the implementation of low-cost, undivided reactors. The anodic generation of bromine is shown in reaction (39). Bromine reacted with water to give hypobromite ions which, in turn, formed propylene oxide via a brominated intermediate (a bromohydrin) in alkaline conditions:

$$HOBr + CH\text{-}CH \rightleftarrows CH_2 + CH_3\text{-}CHOH\text{-}CH_2Br \qquad (44)$$

The cathodic evolution of hydrogen was accompanied by the reverse of reaction (39), i.e., the reduction of bromine to bromide ions.

In a more detailed paper,[30] 1-butene,cis-2-butene,trans-2-butene and ethylene were epoxidised under conditions which gave reasonable yields. The BTTR was made from a glass tube, 30 cm long by 6.5 cm internal diameter, filled with 14 layers of twenty 12.5 mm carbon Raschig rings separated by monofilament nylon meshes, with perforated carbon plates as feeder electrodes. The alignment of successive electrode layers was found to be important. An aligned configuration (Figure 4c) gave a higher space time yield and lower specific energy consumption, as shown in the carpet plot of Figure 11, presumably due to an improved potential distribution down the BTTR. The use of a negative feeder at the top of the tower was also beneficial. The selectivity was high but the current efficiencies were limited to < 65% due to bulk phase chemical reactions being slower than the electrochemical generation of bromine oxidant. Under conditions where the rates of the chemical and electrochemical reactions match, the authors considered that figures of merit would be comparable to those for propylene. During epoxidation, the conformation of each butene isomer was preserved.

Indeed, given the undivided nature of its cells there are other examples of convergent paired electrosynthesis in BTTRs, in which both anodic and cathodic reactions are utilized to form a desirable product.[100] Yet a further series of studies on the effect of type of reactor and their reaction environment on these processes were continued by Johnson and Jansson.[101,102] The work involved the dimerization of methyl acrylate and diethyl malonate in a non-aqueous electrolyte.[101] The BTTR consisted in a 80 mm diameter glass column packed with 10 layers of carbon Raschig rings in a semi-random arrangement (See Figure 4e) and operated in batch recycling mode. The cathodic reaction was the reduction of methyl acrylate into malonate ions and the anodic reaction was the oxidation of iodate. In solution, malonates ion forms a dimer by reacting with iodine or react with methyl acrylate via a Michel addition. After a series of chemical steps, the main products are ethyl dimalonate and dimethyl adipate. Due to the dependence on mixing to achieve a good transport of malonate ions away of the cathode, the pump cell and the capillary gap cell proved superior to the BTTR in terms of reactant conversion. The selectivity improved with higher mixing, reaching up to 85% for ethyl dimalonate and over 90% for dimethyl adipate,[102] showing that mesh separators between the layers of the BTTR can facilitate a useful degree of mixing.

Removal and recovery of metal ions

Metal ions may be removed from low concentration, simple and complex electrolytes at the cathodic zones in the BTTR. Jansson et al.[32] studied batch recirculation of a range of electrolytes through a cylindrical glass tower of 8 cm internal diameter packed with 20-56 bipolar layers of graphite Raschig rings having a diameter of 1.2 cm and a length of 1.0-2.5 cm, the electrode layers being separated by a 1 mm thick mesh. The electrolyte was initially 400 mg dm^{-3} Cu^{2+} + 0.03 mol dm^{-3} H_2SO_4 then a mixed metal solution was used, containing 96 mg dm^{-3} Cu^{2+}, 78 mg dm^{-3} Pb^{2+} and 32 mg dm^{-3} Cd^{2+} in 0.015 mol dm^{-3} HNO_3. Ag(I) ions were studied at an initial 30 mg dm^{-3} Ag concentration in 0.02 mol dm^{-3} sodium thiosulphate. Under these conditions, the electrolyte film thickness on the electrodes, h is estimated to be 0.05 cm. The studies demonstrated that Cu, Ag, Pb and Cd could be removed from a wide range of electrolytes and considered the effect of cell potential difference on the rate of metal ion concentration decay. In particular, the extent of the

side active area of the cathodic zones on each bipolar electrode, θ_L was considered[32] and related to the process conditions. The authors suggested an approximate expression as a scaling law in the batch recirculation mode. Equation (28) could be written:

$$\ln\left[\frac{c_{(t)}}{c_{(0)}}\right] = -\frac{t}{\tau_R}\left[1 - exp\left(\frac{k_m N L_m L_w}{Q} a\right)\right] \quad (45)$$

where the factor *a* allows for the increased electrode area due to a fraction of each layer, θ_L being active and can be expressed as:

$$a = 1 - \left[\frac{\phi_R}{\phi_T}\right] \quad (46)$$

where ϕ_R is the standard potential of the electrode with respect to the counter electrode reaction of oxygen evolution and ϕ_T is the potential difference across one bipole with respect to the counter electrode reaction of oxygen evolution. The expression was valid for Cu, Pb and Ag but not for Cd; this was attributed to the negative electrode potential of cadmium under the experimental conditions resulting in mixed or even charge transfer controlled metal deposition. Values of θ_L ranged from 0.1 to 0.3.

Once deposited, metal can be removed from the BTTR by dissolution in a small volume of electrolyte to produce a concentrate for reuse or further treatment in an electrolytic cell using 2-dimensional electrodes. Three modes of metal recovery from the used BTTR were considered in work by Walsh et al.,[4] at Southampton:

a) open-circuit leaching of the BTTR with no external power supply connected, is simple and minimises power requirements but corrosion may be slow and require dissolved oxygen, i.e., oxygen bubbling, or another oxidant in the case of e.g., copper and nickel.

b) reversal of tower feeder polarity (i.e., reversal of cell potential difference) such that metal deposits become anodic. Metal can be stripped faster but redeposits at new cathodes after a predetermined time.

c) redesign of the tower and electrode packing as a semidisposable cartridge encapsulated in a thin polymer film, allowing furnace refining of precious metals (along with CO_2 scrubbing).

Later, the same researchers employed a pilot commercial BTTR to recover gold from cyanide-based electroplating dragout from 5 dm^3 tanks under the batch recycle mode.[3] The reactor, shown in Figure 8a), incorporated 74 layers of 4 mm thick carbonised perforated fibreboard, each with a 75 cm^2 area and hexagonal shape, affording a total projected cathode area of 0.46 m^2. The BBTR design was improved, being divided in two vertical segments around a flow-across central positive feeder. The two negative feeders were placed at top and bottom of the column. The material used for the feeders was carbon or platinised titanium mesh. The typical operating conditions were 2.3 V per layer (a constant stack voltage of 86 V), a reactor current of 1.8-2.8 A and a volumetric flow rate of 1.0 $dm^3\ min^{-1}$. The reaction at the cathodic sites was:

$$Au(CN)_2^- + 2e^- \rightleftarrows Au + 2CN^- \quad (47)$$

meanwhile, at the anodic sites, cyanide ions were oxidized until the evolution of CO_2:

$$CN^- + 2OH^- - 2e^- \rightleftarrows CNO^- + H_2O \quad (48)$$

$$2CNO^- + 4OH^- - 6e^- \rightleftarrows 2CO_2 + N_2 + H_2 \quad (49)$$

In an electrolyte with a conductivity of up to 22 mS cm^{-1} and a pH 10, the removal efficiency of the initial 4 ppm of gold was approximately 10%, as shown in Figure 8b). The removal efficiency could be improved if layer materials with higher surface area per unit volume were implemented instead of the perforated plates.

The cathodic removal of Cu(II) ions from diluted solutions has also been performed for the analysis and optimization of the operational parameters in BTTRs.[37,58] For instance, Kusakabe et al.[58] determined the contribution of Faradaic and shunt current, allowing them to demonstrate that the removal Cu ions with an initial concentration of 0.01 mol dm^{-3} was up to 30% more efficient in a BTTR when comparison to a packed-bed reactor due to increased shunt currents in the flooded reactor. A lower limit of Cu ion concentration in the electrolyte was 5×10^{-4} mol dm^{-3}, probably due to redissolution. A maximum value of 2.70×10^{-5} m s^{-1} was found for k_m from the fractional conversion over time and a modified equation (28). The BTTR used in this study had a diameter of 66 mm and up to 21 layers of cylindrical ferrite pellets (typically 6 mm in height 6 mm in diameter) separated by 1 mm thick polyethylene net.

Later, Trinidad et al.[37] characterized the mass transport, axial dispersion, residence time and productivity of a Raschig ring BTTR used for the removal of Cu(II) ions during an operating life time of over 11,000 hours. The glass tower contained 57 layers of carbon Raschig rings and had an internal diameter of 7.9 cm and a height of 75 cm. Each bipolar layer comprised 30 rings with a thickness of 1.25 cm and an external diameter of 1.25 cm. The separator was thinner than in other BTTRs, being a 0.5 mm thick polyester mesh of 90% volumetric porosity. Its typical batch recirculation arrangement is shown in Figure 12a). The performance factor k_mA was estimated under constant voltage from the change in Cu(II) concentration in single pass and in batch recirculation modes, using equations (30) and (28), respectively. Initial Cu(II) concentrations of 50, 100, 150 and 200 ppm were considered. It was found that a layer voltage of 2 V was favourable to current efficiency, affording k_mA values of approximately 5.0 cm^3 s^{-1} from the two methods. As shown in Figure 12b), this demonstrated that k_mA values can be estimated within 10% from single pass inlet and outlet concentration measurements, which is useful in technical settings. As shown in Figure 7, the residence time ranged between

9 and 16 minutes as a function of film Reynolds number, which had values between 15 and 45. A maximum current efficiency was 40% for the typical initial concentration of 100 ppm of Cu(II) at a mean linear velocity of 0.68 cm s^{-1}.

Removal of cyanide ions

Jansson et al. considered both direct and indirect oxidation of cyanide ions to cyanate and CO_2 at anodic zones in the BTTR.[33] In the first case, the removal from solution takes place as described in reactions (48) and (49). In the latter case, anodic destruction of cyanide ions was accelerated by addition of chloride ions to the electrolyte, resulting in hypochlorite generation. Complete removal of cyanide ion via indirect hypochlorite generation being represented by:

$$2CN^- + 5HOCl \rightleftarrows 2CO_2 + N_2 + H_2O + 3HCl + 2Cl^- \quad (50)$$

where hypochlorite ion can be formed *in-situ* via hydrolysis of anodically formed chlorine under alkaline conditions, hydroxyl ions being continuously formed via cathodic hydrogen evolution.

$$2H_2O + 2e^- \rightleftarrows H_2 + 2OH^- \quad (51)$$

As shown in Figure 13, El-Ghaoui et al.[33] studied the decay of cyanide ion concentration from an initial level of 300 mg dm^{-3} (ppm) at pH 10.4 during batch recycling of an approx. 2000 cm^3 electrolyte at 0.5-2.0 dm^3 min^{-1} through a BTTR of 7.5 cm internal diameter consisting of 20, 34 or 48 layers of 12.5 mm long, 12.5 mm diameter Raschig rings. The potential difference was 2 or 3 V per layer. The oxidation of cyanide was mass transport controlled being studied as a first order decay of cyanide ion concentration with time. The presence of alkali accelerated the rate of decay, due to hydrolysis of anodically generated chlorine to hypochlorite ion.

Due to pH shifts with time, the authors noted the importance of pH control in practical scale-up. In a related paper, the same authors studied the decay of metal ion concentration during the treatment of heavy metal cyanide solutions in the batch recirculation mode.[35] Figure 14 shows the decrease in concentration of various metal ions as a function of time as they are deposited on the cathodic regions of the tower. The scaling law shown in equation (45) proved useful but behaviour was complicated by the cyanocomplex presence; the ratio of cyanide to metal in solution decreased with time due to anodic oxidation of cyanide.

More recently, Ögütveren et al.[103] demonstrated the performance difference of the same process during single pass and batch recirculation modes. The 22 mm diameter BTTR had 32 layers of graphite Raschig rings with diameters of 6 mm and equal height. Constant potential values of 0.7 to 2.5 V per layer were evaluated, along the effect of pH and background electrolyte concentration. It was found that total removal of cyanide ions could be achieved from initial concentrations of up to 1500 ppm using the batch recycle mode at pH 11 and 2.2. V per layer, from which an average mass transfer coefficient of 4.35×10^{-4} m s^{-1} was calculated. For this case, the maximum energy consumption was 6.3 kW h per kg of cyanide over a period of up to 240 min.

Destruction of organics

The main application of BTTRs for environmental treatment consists in the removal of many organic pollutants, including persistent dyes, from industrial process liquors or from treated waters. These operations can proceed by direct anodic oxidation at a surface electrocatalyst[104,105] or via indirect 'advanced oxidation', i.e. the reaction with solution borne electrogenerated radicals,[61,106,107] which may involve Fe^{3+} in a Fenton oxidation or an electrochemically regenerated oxidant, including an oxyanion, ozone, a chlorine species or a cocktail of oxidants. In the first case, the desired reaction is heterogeneous in nature, whereas in the latter the electrode process is enhanced by a homogenous reaction.[106]

Direct anodic oxidation can be slow and improved by a suitable electrocatalyst, often promoting hydroxyl radical formation.[107,108] In a simple classification, Comninellis et al.[104,105] have distinguished between two types of electrocatalyst:

a) electrodes that act only as an inert surface (e.g. Pt, IrO_2 and RuO_2) or

b) electrode surfaces which participate chemically in anodic oxidations, e.g., via oxygen donation, oxygen evolution and bonding with oxygen (such as PbO_2,[109,110] SnO_2, MnO_2 or BDD[40,111]).

There is a research opportunity in revisiting the direct degradation of organics in BTTRs employing high surface area BDD electrodes at the bipolar layers under trickle flow. Indeed, further work by Ögütveren et al. can be taken as inspiration since they presented a series of bipolar packed bed reactors employing niobium-coated BBD Raschig rings under the designation of 'BTTRs'. As mentioned above, an upward flow within a flooded tower, hence without a falling thin electrolyte film, is not a characteristic of true BTTRs. These devices, described in detail in references [38] and [46], were used for the degradation Basic Red 29,[38] Basic Blue 3,[47] and Reactive Black 5 textile dyes,[21] along phenol[46] and mixed petroleum refinery effluents.[48] Hydroxyl radicals formed at the electrodes played a central role to the oxidation mechanisms.[107,108]

Over the last decade, indirect anodic oxidations, often with Fenton oxidations, have increasingly been applied to the removal of synthetic and real organic dye contaminants in wastewater. Such dyes are often environmentally persistent and stable, requiring 'advanced oxidation processes' (AOP) to decolourise them.[109] Unfortunately, there has been a tendency in the literature to be vague about the active oxidant and the role of electrochemistry. Indeed, some oxidations are complex, involving multiple oxidants, direct and indirect anodic oxidations and several mediators together with electrocatalysts.

Some examples of indirect anodic dye decolourisation in BTTRs involving the electrogeneration of chlorine species at the trickling thin film during batch recycle operation have been given by Ögütveren et al. For

instance, the indirect decolourization of Congo Red and Xiron Blau 2RHD dyes was performed in a NaCl electrolyte.[18] By controlling the pH of the solution, Cl_2, HOCl or OCl^- could be produced. The BTTR had an internal diameter of 22 mm and comprised 27 bipolar layers formed by four 6 mm × 6 mm graphite Raschig rings. As shown in Figure 15, the removal efficiency in this BTTR reached up to 93% for Congo Red and 97% for Xiron Blau 2RHD from initial dye concentrations of 30 and 40 ppm, respectively. Recommended potential values at the individual layers fell between 1.5 and 1.8 V and flow rates of up to 396 $cm^3\ h^{-1}$. The maximum energy consumption was 0.056 kW h g^{-1} for Congo Red and 0.031 kW h g^{-1} for Xiron Blau 2RHD. A subsequent work focused on the destruction of Ostazin Red H3B, Ostazin Black HN and Ostazin Olive HG textile dyes using the same BTTR under equivalent flow rates and layer potential.[112] Maximum removal efficiencies of 98%, 70% and 85% were achieved for Ostazin Red H3B, Ostazin Black HN and Ostazin Olive HG, respectively. The initial pH of the solutions was also neutral and the initial concentration was 40 ppm in the first case and 30 ppm in the latter two. The energy consumption ranges between 0.029 and 0.044 kW h g^{-1}. Unfortunately, no current efficiency values are given in the above studies, nor is the linear velocity of electrolyte past the electrode surface stated.

Other uses

While electrosynthesis and environmental treatment have been the main applications area for the BTTR, important specialised applications have involved or proposed:

a) removal of microbial contamination from liquids in e.g. the treatment of cooling tower waters, [113]

b) combined chemical, electrochemical and electrophoretic adsorption/desorption of metal ions (Pt group, Au, Ag) using activated carbon cloth/packed granular bed/carbonised perforated fibreboard layers,[4]

c) The synthesis of peroxide in alkaline solution in modified BTTRs[49] and packed bed electrode reactors,[52]

d) Water purification and disinfection via peroxide and hypochlorite generation in the BTTR,[106]

e) Electrocoagulation of Acilan Blau dye using soluble steel Raschig rings from slightly alkaline textile industry effluents.[36]

Conclusions

1. The BTTR concept involves trickle flow of a thin film of electrolyte, under gravity, down a packed column of identical, electrically separate, porous 3D, bipolar electrode layers. Up to 100 identical, bipolar layers may be involved. The bipolar electrode layers experience a thin film of electrolyte via gravity trickle flow down an insulating polymeric or glass column.

2. Compared to packed bed reactors, the BTTR has a lower pressure drop and allows improved gas disengagement its construction is simpler and easier to replicate and lower in cost than flow through, undivided bipolar mesh reactors.

3. The benefits of the BTTR include simplicity of construction and electrical connections, the ability to offer an alternating polarity environment and facility to handle solutions of relatively low conductivity. Limitations include electrodes needing to be configured in a suitable form, the inability to incorporate membranes, the need to avoid excessive bypass currents inside (and outside) the tower, hence electrolytes should not have too high a conductivity.

4. Construction of the BTTR has followed three generic formats, as the reactor has developed to meet industrial, production and scale-up needs. The first design, which was used for diverse laboratory studies of reaction environment, incorporated organised layers of individual Raschig rings in a circular, glass column with top and bottom electrical feeder. The second design used a transformational approach with heat-shrunk plastic encapsulation of diverse, porous electrode materials incorporating a central, back-to back current feeder with top and bottom feeders having the same polarity to suit an industrial prototype for metal removal from wastes. Finally, digitally designed and 3D printed electrodes and separators may be integrated into a polymeric column for future and diversifying designs and application sectors.

5. Electrode choice for the packing material has evolved from horizontal layers of carbon Raschig rings through various one-piece or multiple carbon or metal particle layers/meshes/foams through to 3D printed mesh/foam/separator-column constructions.

6. The alternating potential field down the tower provides a unique reaction environment facilitating, e.g. anodic breakdown of inorganic complexes followed by cathodic deposition of metal or the complete oxidation of persistent organic complexes.

7. In global terms, the performance of the BTTR can be often be modelled as a PFR having a total electrode area and an averaged mass transport coefficient. These parameters are readily found from a simple batch recirculation study on a known volume of a particular electrolyte. In microscopic terms, the reaction environment down the tower can be viewed as a zoned reactor model having anodic, cathodic and inactive zones. The active electrode area is dependent on electrolyte composition, stack potential difference and operational conditions.

8. Scale-up of the BTTR can be achieved in several ways (which have limitations):

a) Incorporation of more bipolar electrode layers (which leads to higher stack voltages, hence health and safety concerns together with difficulties sourcing a suitable direct current power supply).

b) Use of a larger projected area electrode layer (which can become heavy and present difficulties in achieving uniform electrolyte distribution without additional flow inlet distributors).

c) Deployment of porous, 3D electrode materials (which must have sufficiently uniform electrolyte flow, potential and current distributions across each layer).

9. Unfortunately, few studies over the last decade have stated, or been aware, of the importance of electrolyte flow velocity to reactor performance; some studies only state a volumetric flow rate. Information on the volumetric porosity of the electrode packing is also rare; many studies do not state the volumetric electrode area or averaged mass transfer coefficient under convective-diffusion controlled reaction conditions.

10. The application areas for the BTTR include environmental treatment (metal ion removal, oxidation of organics including decolourisation of synthetic organic dyes (e.g., methyl orange and azo-dyes) together with generation of peroxy species), synthesis of organics (e.g., epoxidation of alkenes, methoxylation of furan), plus regeneration of inorganic catalysts (such as Co(III) acetate).

Recommendations for further work

A number of aspects of BTTR construction, operation and performance deserve further R & D endeavour:

1. Novel, economical, long lifetime and sustainable packing materials, both supports and catalysts, which are resistant to corrosion.

2. 3D printed versions of both the porous electrodes layers and the separators as well as fast prototyping techniques for outer tower fabrication.

3. The use of interdigitated electrodes with thin layer electrolyte flow provide a strategy for a new generation of tailored and microflow BTTRs capable of facile scale-up.

4. The relative performance when treating real industrial electrolytes containing *mixed* metal complexes and additives at varying pH.

5. Relative performance when treating electrolytes containing *mixtures* of organic dyes in real electrolytes, rather than single dyes in synthetic solutions.

6. Characterisation of reaction environment (including active area, flow dispersion, mass transfer and potential distribution) in modern porous, 3D porous materials as layers in BTTRs.

7. The rigorous application of figures of merit describing performance, to facilitate comparisons between packing materials or between the BTTR and competitive reactors.

8. Developing film Reynolds number expressions for the trickle flow on contemporary materials beyond Rashig rings, such as meshes, foams and felts.

9. Developing numerical simulations of the hydrodynamic and electrochemical behavior of BTTRs.

10. Consideration of implementing electrochemical BTTRs at high pressure and high temperatures, where they can offer design simplicity and high reliability.

Acknowledgements

FCW gratefully acknowledges early encouragement to improve the construction of the bipolar trickle tower reactor and its reaction environment by M. Fleischmann, R.E.W. Jansson and D.J. Schiffrin. Assistance with chemical analysis during early studies was provided by F.M. Lesch. The British Technology Group provided funding to assist studies carried out at the Wolfson Centre for Electrochemical Sciences, Chemistry Department at the University of Southampton, UK. The Metelec Co, Hastings collaborated in the early construction of a prototype BTTR for industrial gold recovery from electroplating rinse waters, which was evaluated on-site, at Pender Plating, Poole, UK.

References

1. L. F. Arenas, C. Ponce de León, and F. C. Walsh, *J. Electrochem. Soc.*, **167**, 023504 (2020).

2. M. Fleischmann, C. J. H. King, J. W. Oldfield, R. E. Plimley, and C. L. K. Tennakoon, (1971).

3. F. C. Walsh and G. W. Reade, in *Environmental Oriented Electrochemistry*, Studies in Environmental Science. vol. 59, p. 3–44, Elsevier (1994).

4. F. M. Lesch, F. C. Walsh, and D. J. Schiffrin, Unpuplished (1982).

5. A. K. Saroha and K. D. P. Nigam, *Reviews in Chemical Engineering*, **12**, 207–347 (1996).

6. J. R. Backhurst, J. H. Harker, J. F. Richardson, and J. M. Coulson, *Chemical Engineering, Fluid Flow, Heat Transfer and Mass Transfer* R. P. Chhabra, Editor, 6 ed., Elsevier, (1999).

7. D. J. Pickett, *Electrochemical Reactor Design*, 2nd ed., Elsevier, Amsterdam, (1979).

8. F. Goodridge, *Phil. Trans. R. Soc. Lond. A*, **302**, 275–284 (1981).

9. F. Coeuret and A. Storck, *Eleménts de Génie Electrochimique, Techniques et Documentation*, 1st ed., Lavoisier, (1984).

10. R. J. Marshall and F. C. Walsh, *Surface Technology*, **24**, 45–77 (1985).

11. E. Heitz and G. Kreysa, *Principles of Electrochemical Engineering*, p. 1, VHC, Weinheim, (1986).

12. F. Goodridge and K. Scott, *Electrochemical Process Engineering*, p. 1, Springer Science & Business Media, New York, (1995).

13. D. Pletcher and F. C. Walsh, *Industrial Electrochemistry*, 2nd ed., Chapman and Hall, London, (1990).

14. F. C. Walsh and G. Reade, *Analyst*, **119**, 791–6 (1994).

15. F. C. Walsh and G. Reade, *Analyst*, **119**, 797–7 (1994).

16. S. Bebelis et al., *Trans. IChemE*, **91**, 1998–2020 (2013).

17. F. C. Walsh and D. Pletcher, in *Developments in Electrochemistry: Science Inspired by Martin Fleischmann*, D. Pletcher, Z.-Q. Tian, and D. Williams, Editors, p. 95–111, John Wiley & Sons (2014).

18. Ü. B. Öğütveren and S. Koparal, *Int. J. Environmental Studies*, **42**, 41–52 (1992).

19. F. C. Walsh and C. Ponce de León, *Electrochim. Acta*, **280**, 121–148 (2018).

20. L. F. Arenas, C. Ponce de León, and F. C. Walsh, *Curr. Opin. Electrochem.*, **16**, 1–9 (2019).

21. Y. Yavuz and R. Shahbazi, *Sep. Pur. Technol.*, **85**, 130–136 (2012).

22. C. Ponce de León et al., *Chem. Eng. Trans.*, **41**, 1–6 (2014).

23. L. F. Arenas, F. C. Walsh, and C. Ponce de León, *ECS J. Solid State Sci. Technol.*, **4**, P3080–P3085 (2015).

24. L. F. Arenas, C. Ponce de León, and F. C. Walsh, *Electrochem. Commun.*, **77**, 133–137 (2017).

25. A. Attour et al., *Chem. Eng. Sci.*, **66**, 480–489 (2011).

26. M. J. Orella, Y. Román-Leshkov, and F. R. Brushett, *Current Opinion in Chemical Engineering*, **20**, 159–167 (2018).

27. M. Fleischmann and R. E. W. Jansson, *Chemie Ingenieur Technik*, **49**, 283–287 (1977).

28. M. Fleischmann and Z. Ibrisagić, *J. Appl. Electrochem.*, **10**, 157–168 (1980).

29. A. V. Boussoulengas, S. Ehdaie, and R. E. W. Jansson, *Chemistry and Industry*, **6**, 670–672 (1979).

30. K. G. Ellis and R. E. W. Jansson, *J. Appl. Electrochem.*, **11**, 531–535 (1981).

31. M. Fleischmann and Z. Ibrisagić, *J. Appl. Electrochem.*, **10**, 151–156 (1980).

32. S. Ehdaie, M. Fleischmann, and R. E. W. Jansson, *J. Appl. Electrochem.*, **12**, 59–67 (1982).

33. E. A. El-Ghaoui, R. E. W. Jansson, and C. Moreland, *J. Appl. Electrochem.*, **12**, 69–73 (1982).

34. K. G. Ellis and R. E. W. Jansson, *J. Appl. Electrochem.*, **13**, 657–661 (1983).

35. E. A. El-Ghaoui and R. E. W. Jansson, *J. Appl. Electrochem.*, **12**, 75–80 (1982).

36. Ü. B. Öğütveren, N. Gönen, and S. Koparal, *Journal of Environmental Science and Health . Part A: Environmental Science and Engineering and Toxicology*, **27**, 1237–1247 (1992).

37. P. Trinidad, F. C. Walsh, S. A. Sheppard, S. P. Gillard, and S. A. Campbell, *J. Chem. Technol. Biotechnol.*, **79**, 954–960 (2004).

38. A. S. Koparal, Y. Yavuz, C. Gürel, and Ü. B. Öğütveren, *J. Hazard. Mater.*, **145**, 100–108 (2007).

39. O. González Pérez and J. M. Bisang, *J. Appl. Electrochem.*, **40**, 709–718 (2010).

40. E. Brillas and C. A. Martínez-Huitle, *App. Catal. B: Environ.*, **166-167**, 603–643 (2015).

41. J. L. Nava and C. Ponce de León, in *Electro-Fenton. Process New Trends and Scale-Up*, M. Zhou, M. A. Oturan, and I. Sirés, Editors, p. 263–286, Springer, Singapore (2017).

42. L. Cedheim, L. Eberson, B. Helgee, K. N. A. Chem, and R. E. Plimley, *Acta Chem. Scand. B*, **29**, 617–621 (1975).

43. C. Belmont, thesis, PhD Thesis, The University of Edinburgh (1994).

44. F. Beck, *J. Appl. Electrochem.*, **2**, 59–69 (1972).

45. J.-Y. Jeong, H.-K. Kim, J.-H. Kim, and J.-Y. Park, *Chemosphere*, **89**, 172–178 (2012).

46. Y. Yavuz, A. S. Koparal, and Ü. B. Öğütveren, *J. Environ. Eng.*, **134**, 24–31 (2008).

47. Y. Yavuz, A. Savaş Koparal, and Ü. B. Öğütveren, *J. Chem. Technol. Biotechnol.*, **86**, 261–265 (2010).

48. Y. Yavuz, A. S. Koparal, and Ü. B. Öğütveren, *Desalination*, **258**, 201–205 (2010).

49. C. Oloman and A. P. Watkinson, *J. Appl. Electrochem.*, **9**, 117–123 (1979).

50. A. Manji and C. W. Oloman, *J. Appl. Electrochem.*, **17**, 532–544 (1987).

51. C. Oloman, Ben Lee, and W. Leyten, *Can. J. Chem. Eng.*, **68**, 1004–1009 (1990).

52. N. Gupta and C. W. Oloman, *J. Appl. Electrochem.*, **36**, 1133–1141 (2006).

53. K. Kusakabe, S. Morooka, and Y. Kato, *J. Chem. Eng. Japan*, **15**, 45–50 (1982).

54. K. Kusakabe, T. Kimura, S. Morooka, and Y. Kato, *J. Chem. Eng. Japan*, **17**, 293–297 (1984).

55. R. Zhu, C. Yang, M. Zhou, and J. Wang, *Chem. Eng. J.*, **260**, 427–433 (2015).

56. M. Sudoh, H. Kamei, and K. Koide, *J. Chem. Eng. Japan*, **18**, 148–153 (1985).

57. L. Franke, A. Zimmer, and K. Seibig, *Chemie Ingenieur Technik*, **64**, 652–653 (1992).

58. K. Kusakabe, T. Kimura, S. Morooka, and Y. Kato, *J. Appl. Electrochem.*, **17**, 724–730 (1987).

59. J. R. Smith, F. C. Walsh, and R. L. Clarke, *J. Appl. Electrochem.*, **28**, 1021–1033 (1998).

60. F. C. Walsh and R. G. A. Wills, *Electrochim. Acta*, **55**, 6342–6351 (2010).

61. O. M. Cornejo, M. F. Murrieta, L. F. Castañeda, and J. L. Nava, *Electrochim. Acta*, **331**, 135373 (2020).

62. K. Kugler, M. Luhn, J. A. Schramm, K. Rahimi, and M. Wessling, *Phys. Chem. Chem. Phys.*, **17**, 3768–3782 (2015).

63. L. F. Arenas, C. Ponce de León, R. P. Boardman, and F. C. Walsh, *J. Electrochem. Soc.*, **164**, D57–D66 (2017).

64. D. C. Dunand, *Advanced Engineering Materials*, **6**, 369–376 (2004).

65. L. Lipp and D. Pletcher, *Electrochim. Acta*, **42**, 1101–1111 (1997).

66. L. F. Arenas, C. Ponce de León, R. P. Boardman, and F. C. Walsh, *Electrochim. Acta*, **247**, 994–1005 (2017).

67. P. Lettenmeier et al., *Sci. Rep.*, **7**, 44035 (2017).

68. H. Schäfer and M. Chatenet, *ACS Energy Lett.*, **3**, 574–591 (2018).

69. X. Tian and K. Zhou, *Nanoscale*, **12**, 7416–7432 (2020).

70. F. C. Walsh, L. F. Arenas, and C. Ponce de León, *Trans. IMF.*, **98**, 65–72 (2020).

71. L. F. Arenas, N. Kaishubayeva, C. Ponce de León, and F. C. Walsh, *Trans. IMF.*, **98**, 48–52 (2020).

72. L. F. Castañeda, F. C. Walsh, J. L. Nava, and C. Ponce de León, *Electrochim. Acta*, **258**, 1115–1139 (2017).

73. J. M. Friedrich, C. Ponce de León, G. W. Reade, and F. C. Walsh, *J. Electroanal. Chem.*, **561**, 203–217 (2004).

74. F. C. Walsh et al., *Electrochim. Acta*, **215**, 566–591 (2016).

75. P. Wang et al., *Adv. Mater. Technol.*, **5**, 1901030–11 (2020).

76. R. Jansson and N. R. Tomov, *Fuel Process. Technol.*, **25**, 497–503 (1980).

77. D. Prando et al., *JABFM*, **15**, e291–e302 (2017).

78. P. C. S. Hayfield, *Platinum Metals Rev.*, **42**, 46–55 (1998).

79. P. A. Christensen et al., *Ozone Sci. Eng.*, **31**, 287–293 (2009).

80. R. A. Márquez-Montes et al., *ACS Sustainable Chem. Eng.*, **8**, 3896−3905 (2020).

81. A. Bandyopadhyay and B. Heer, *Materials Science and Engineering: R: Reports*, **129**, 1–16 (2018).

82. K. Scott, *Renew. Sust. Energ. Rev.*, **81**, 1406–1426 (2018).

83. K. Nandakumar, Y. Shu, and K. T. Chuang, *AIChE J.*, **45**, 2286–2297 (1999).

84. S. Langlois and F. Coeuret, *J. Appl. Electrochem.*, **19**, 43–50 (1989).

85. P. Pichaichanarong, R. M. Spotnitz, R. P. Kreh, S. M. Goldfarb, and J. T. Lundquist, *Chem. Eng. Commun.*, **94**, 119–130 (2007).

86. J. González-García et al., *Ind. Eng. Chem. Res.*, **39**, 1132–1142 (2000).

87. G. Aparicio-Mauricio, F. A. Rodríguez, J. J. H. Pijpers, M. R. Cruz-Díaz, and E. P. Rivero, *J. Energy Storage*, **29**, 101337 (2020).

88. O. Levenspiel and W. K. Smith, *Chem. Eng. Sci.*, **6**, 227–235 (1957).

89. M. Fleischmann and Z. Ibrisagić, *J. Appl. Electrochem.*, **10**, 169–172 (1980).

90. M. Fleischmann and R. E. W. Jansson, *J. Chem. Technol. Biotechnol.*, **30**, 351–358 (1980).

91. A. Souadnia, F. Soltana, F. Lesage, and M. A. Latifi, *Chemical Engineering and Processing: Process Intensification*, **44**, 847–854 (2005).

92. M. A. Latifi, A. Naderifar, and N. Miidoux, *Trans. IChemE*, **77**, 69–73 (1999).

93. G. Kreysa, *Electrochim. Acta*, **26**, 1693–1694 (1981).

94. F. C. Walsh, *Electrochim. Acta*, **38**, 465–468 (1993).

95. A. Güvenç, B. Karabacakoglu, Ö. M. Koçkar, and A. T. Pekel, *Turk. J. Chem.*, **24**, 101–108 (2000).

96. Ü. B. Öğütveren, R. E. Plimley, and I. Nieva, *J. Appl. Electrochem.*, **22**, 351–357 (1992).

97. A. Güvenç, A. T. Pekel, and Ö. M. Koçkar, *Chem. Eng. J.*, **99**, 257–263 (2004).

98. D. E. Danly and C. R. Campbell, in *Techniques of Electroorganic Synthesis (techniques of chemistry, volume V) Part III. Scale-Up and Engineering Aspects*, N. L. Weinberg and B. V. Tilak, Editors, p. 284–384, Technique of Electroorganic Synthesis (1982).

99. N. R. Tomov and R. E. W. Jansson, *J. Chem. Technol. Biotechnol.*, **30**, 110–116 (1980).

100. N. Aust and A. Kirste, in *Encyclopedia of Applied Electrochemistry*,, p. 1505–1510, Springer, New York, NY, New York (2014).

101. D. K. Johnson and R. E. W. Jansson, *J. Chem. Technol. Biotechnol.*, **30**, 200–204 (1980).

102. D. K. Johnson and R. E. W. Jansson, *J. Electrochem. Soc.*, **128**, 1885–6 (1981).

103. Ü. B. Öğütveren, E. Törü, and S. Koparal, *Water Res.*, **33** (1999).

104. C. Comninellis, *Electrochim. Acta*, **39**, 1857–1862 (1994).

105. C. Comninellis and A. De Battisti, *J. Chim. Phys.*, **93**, 673–679 (1996).

106. I. Sirés and E. Brillas, in *Evaluation of Electrochemical Reactors as a New Way to Environmental Protection*, J. M. Peralta-Hernández, M. A. Rodrigo-Rodrigo, and C. A. Martínez-Huilte, Editors, p. 57–76, Research Signpost, Kerala (2014).

107. P. V. Nidheesh, M. Zhou, and M. A. Oturan, *Chemosphere*, **197**, 210–227 (2018).

108. M. Panizza and G. Cerisola, *Chem. Rev.*, **109**, 6541–6569 (2009).

109. I. Sirés, C. T. J. Low, C. Ponce de León, and F. C. Walsh, *Electrochem. Commun.*, **12**, 70–74 (2010).

110. X. Li, D. Pletcher, and F. C. Walsh, *Chem. Soc. Rev.*, **40**, 3879–3894 (2011).

111. J. M. Peralta-Hernández, M. Méndez-Tovar, R. Guerra-Sánchez, C. A. Martínez-Huitle, and J. L. Nava, *International Journal of Electrochemistry*, **2012**, 1–18 (2012).

112. Ü. B. Öğütveren and S. Koparal, *Journal of Environmental Science and Health . Part A: Environmental Science and Engineering and Toxicology*, **29**, 1–16 (1994).

113. S. A. Campbell and F. C. Walsh, Unpublished work (2004).

114. C. Belmont and H. H. Girault, *J. Appl. Electrochem.*, **24**, 719–724 (1994).

Electrode material packing in the tower	Total number of layers, N	Number of electrode elements per layer, N_e	Internal cross-sectional area of tower, A_x / cm^2	Length of the tower, L / cm	Total weight of packing / g	Indicative cost per unit electrode packing weight / £ kg^{-1}
Raschig Ring (hollow, vertical cylinders)	58	30	49	75	3,200	2,160
Rectangular rods	20	23	185	25	4,295	630
Carbon cloth	91	1	17.4	11	42	14,600
Solid fuel particles	19	numerous	17.4	11.3	115	0.3
Granulated carbon	24	numerous	26	14	272	6

Table 1. Diverse carbon electrode packing materials used in BTTRs and their averaged performance for mass transport controlled removal of cupric ion from an acid sulphate solution with an initial concentration of 100 mg dm^{-3} of Cu^{2+} ion at 22°C. Reproduced with permission from Walsh and Ponce de León, 2018, Progress in electrochemical flow reactors for laboratory and pilot scale processing. *Electrochimica Acta*, 280, p. 121-148.[19] Data initially taken from Lesch et al.[4]

Figure captions

Figure 1 The bipolar trickle tower reactor concept, in which a thin film of electrolyte flows down a column past a series of identical bipolar electrode layers.

Figure 2 A timeline showing selected developments in the bipolar trickle tower reactor. Initial patent on the BTTR (1971);[2] Fluid flow and mass transfer studies (1972-1979);[27,28] Electrosynthesis of propylene oxide (1979);[29,30] Electrode potential studies (1980);[31] Metal ion removal from synthetic effluent (1981);[32] Anodic oxidation of cyanide from wastewater (1982);[33] Epoxidation of ethylene and butene (1983);[34] Combined cathodic metal deposition and cyanide removal from waste solutions (1983);[35] Redesign of the BTTR, including different electrode forms (1982-1985);[3,4] Precious metal recovery (1986);[3,4] Degradation of textile dyes dye at electrode surface (1992);[18] Electrocoagulation with soluble electrodes (1992);[36] Study of operational parameters in a 22-year duty BTTR;[37] (2004); Bipolar BDD Raschig rings (2007);[38] Mathematical modelling of 3D bipolar electrodes (2010);[39] Review of electrochemical decontamination of wastewater from organics (2015);[40] Review of electrochemical reactor design for advanced oxidation (2017).[41] Revisiting the BTTR with modern high-surface area electrodes (including 3D printed) for sustainable applications.

Figure 3 Concepts for thin film electrolyte and bipolar electrode reactors. a) Monopolar concentric capillary gap (Eberson) cell,[42] b) flow over monopolar interdigitated band electrodes,[114] c) bipolar stacked disc, capillary radial outflow (Beck) cell[44] and d) bipolar packed bed cell.[45]

Figure 4 The arrangement of Raschig ring electrodes in a BTTR a) hexagonally closed packed and b) randomly packed in succession, c) in-line, d) random or semi-random layers vertically down the tower. After Ellis and Jansson.[30]

Figure 5 Types of electrodes used in the BTTR. a) carbon or metal Raschig rings, b) titanium mesh, c) graphite granules, d) carbon or metal foam, e) titanium felt, and f) perforated carbon plate. Metal substrates can be coated with a catalyst such as platinum or BBD.

Figure 6 The zoned behaviour of the BTTR. a) the progress of electrolyte down the reactor involves an entry (inlet and flow conditioning) zone, the bipolar stack of electrodes separated by plastic

meshes in the tower packing, then a drainage, outlet zone, b) an individual cell is formed between electrode layers across a thin electrolyte film in the region of the polymer mesh separator, c) an individual bipolar layer can be divided into 3 regions. At very negative overpotential at the top edge, a cathodic region exists; at the opposite, lower end of there is an anodic region; a central zone of the layer having little or no electrochemical activity, d) in a simple, black-box approach, the BTTR can be viewed as a single pass PFR experiencing a steady volumetric flow rate, Q resulting in a mean linear velocity, v of electrolyte, with the inlet reactant concentration at the top, $c_{(in)}$ progressively falling to the outlet concentration, $c_{(out)}$ at the bottom.

Figure 7 Mean residence time measurements in a Raschig ring BTTR as a function of film Re number. Solid circles: actual values calculated from analysis of the first moment of KCl concentration *vs*. time curves. Solid squares: nominal values calculated from the relationship: $\tau_R = V_R/Q$. Reproduced with permission from Trinidad et al., 2004, The effect of operational parameters on the performance of a bipolar trickle tower reactor. *J. Chem. Technol. Biotechnol.* 79(9), p. 954-960.[37]

Figure 8 A laboratory BTTR (1982) for environmental treatment of dilute, aqueous electrolytes. a) An improved 3-feeder configuration and disposable cartridges of electrode packings.[4] b) Concentration decay of gold and cyanide ions during the processing of a 5 dm^3 volume of a gold cyanide electroplating rinse at 22°C from an initial concentration of 42 mg dm^{-3} gold; data taken from.[3] Adapted with permission from Walsh and Ponce de León., 2018, Progress in electrochemical flow reactors for laboratory and pilot scale processing. *Electrochim. Acta*, 280, p. 121-148.[19]

Figure 9 An example of the simulation of bipolar 3D electrodes in a flooded, vertical reactor which could be adapted for BTTRs. a) Diagram of a stack with a single bipolar porous electrode. *A*, terminal anode; *B*, bipolar electrode; *C*, terminal cathode. The current at the metal (I_m) and solution phases (I_s) is represented schematically as a function of the distance along the bipolar layer (L). b) Simulated leakage current fraction (Ψ_{th}) for increasing cell current (I). Adapted with permission from González Perez and Bisang, 2010, Theoretical and experimental study of electrochemical reactors with three-dimensional bipolar electrodes. *J. Appl. Electrochem.*, 40, p. 709-718.[39]

Figure 10 Application of the BTTR to electrosynthesis of cobalt compounds. Change in the space-time yield with current per layer of rings for initial Co(II) concentrations of: a) 50 mol m^{-3} and b) 100 mol m^{-3} of Co(II) ions at different mean linear flow velocity of electrolyte falling past the electrode surface. Closed circles: 6.7×10^{-2}; open circles: 2.0×10^{-2}; open triangles: 1.34×10^{-2}; closed triangles: 4.0×10^{-2} cm s^{-1}. Adapted with permission from Ogutveren et al., 1992, The behaviour of a trickle tower electrolytic cell for the production of cobalt(III) acetate from cobalt(II) acetate. *J. Appl. Electrochem.*, 22, p. 351-357.[96]

Figure 11 Application of the BTTR to electrosynthesis. The effects of polarity and sodium bromide concentration on performance of a BTTR used for synthesis of propylene oxide. *A* (upper curve) and *B* (lower curve) denote the polarity. The carpet plot shows space time yield *vs.* specific energy consumption. After 60 recycles of electrolyte. Q = 500 cm^3 min^{-1}; 3.5 V per layer; 1% NaBr. Open circles: aligned layer configuration; closed circle (one point): staggered arrangement. Adapted with permission from Ellis and Jansson, 1981, Further studies on the epoxidation of propylene in a bipolar trickle bed. *J. App. Electrochem.*, 11, p. 531-535.[30]

Figure 12 A Raschig ring laboratory BTTR for the study of operational parameters. a) Experimental arrangement. *a*, magnetically-coupled pump; *b*, by-pass valve; c, water-cooled glass coil condenser; *d*, flow control valve; *e*, rotameter; *f*, carbon electrode packing material; *g*, electrolyte reservoir (3 dm^3); *h*, direct current power supply (200 V/10 A); *i*, tower. b) Inlet and outlet concentrations from the BTTR for Cu(II) ion removal from acid sulphate solution at pH 2 as a function of time at 2.0 V per layer, Q = 33.3 cm^3 s^{-1} and $c_{(0)}$ = 100 mg dm^{-3}. Reproduced with permission from Trinidad et al., 2004, The effect of operational parameters on the performance of a bipolar trickle tower reactor. *J. Chem. Technol. Biotechnol.* 79(9), p. 954-960.[37]

Figure 13 Application of the BTTR to cyanide oxidation. Concentration decay of cyanide ion during batch recycling of an approx. 2000 cm^3 volume at 0.5, 1.0, 1.5 and 2.0 dm^3 min^{-1} through the BTTR of 7.5 cm internal diameter, which consisted of 20, 34 or 48 layers of 12.5 mm long, 12.5 mm diameter Raschig rings, operated at 2 or 3 V per layer. Initial CN^- concentration: 300 mg dm^{-3} (ppm) at pH 10.4. Closed squares: 49 layers, 3 V/layer, 2 dm^3 min^{-1}; open circles: 49 layers, 3 V/layer, 0.5 dm^3 min^{-1}; solid triangles: 21 layers, 2 V/layer, 1.0 dm^3 min^{-1}; open circles: 21 layers, 2 V/layer, 0.5 dm^3 min^{-1}. Reproduced with permission from El-Ghaoui et al., 1982,

Application of the trickle tower to problems of pollution control. II. The direct and indirect oxidation of cyanide. *J. Appl. Electrochem.*, 12, p. 69-73.[33]

Figure 14 Application of the BTTR to environmental remediation of Zn, Ni, Cu, Pb and Cd and cyanide removal from metal cyanide complex solutions. Concentration decay during batch recycling of an approx. 1000 cm^3 volume at 0.6 dm^3 min^{-1} through the BTTR of 6.2 cm internal diameter, which consisted of 7 layers of 6.5 mm long, 6.5 mm diameter Raschig rings, operated at 2.25 V per layer. Initial metal and CN^- concentrations were 100 and 300 mg dm^{-3} (ppm) at pH 10. Reproduced with permission from El-Ghaoui and Jansson, 1982, Application of the trickle tower to problems of pollution control. III. Heavy-metal cyanide solutions. *J. Appl. Electrochem.*, 12, p. 75-80.[35]

Figure 15 Removal rate of textile dyes vs. applied potential at different volumetric flow rates for a BTTR with an internal diameter of 22 mm and 27 bipolar layers formed by four 6 mm × 6 mm graphite Raschig rings. a) For Congo Red. b) For Xiron Blau 2RHD. Open squares: 1.38×10^{-4} m^3 h^{-1}; solid squares: 2.28×10^{-4} m^3 h^{-1}; solid diamonds: 3.12×10^{-4} m^3 h^{-1}; open diamonds: 3.96×10^{-4} m^3 h^{-1}. Data taken from Ögütveren and Koparal, 1992, Electrochemical treatment of water containing dye-stuffs: anodic oxidation of Congo Red and Xiron Blau 2RHD. *Intern. J. Environmental Studies*, 42, p. 41-52.[18]

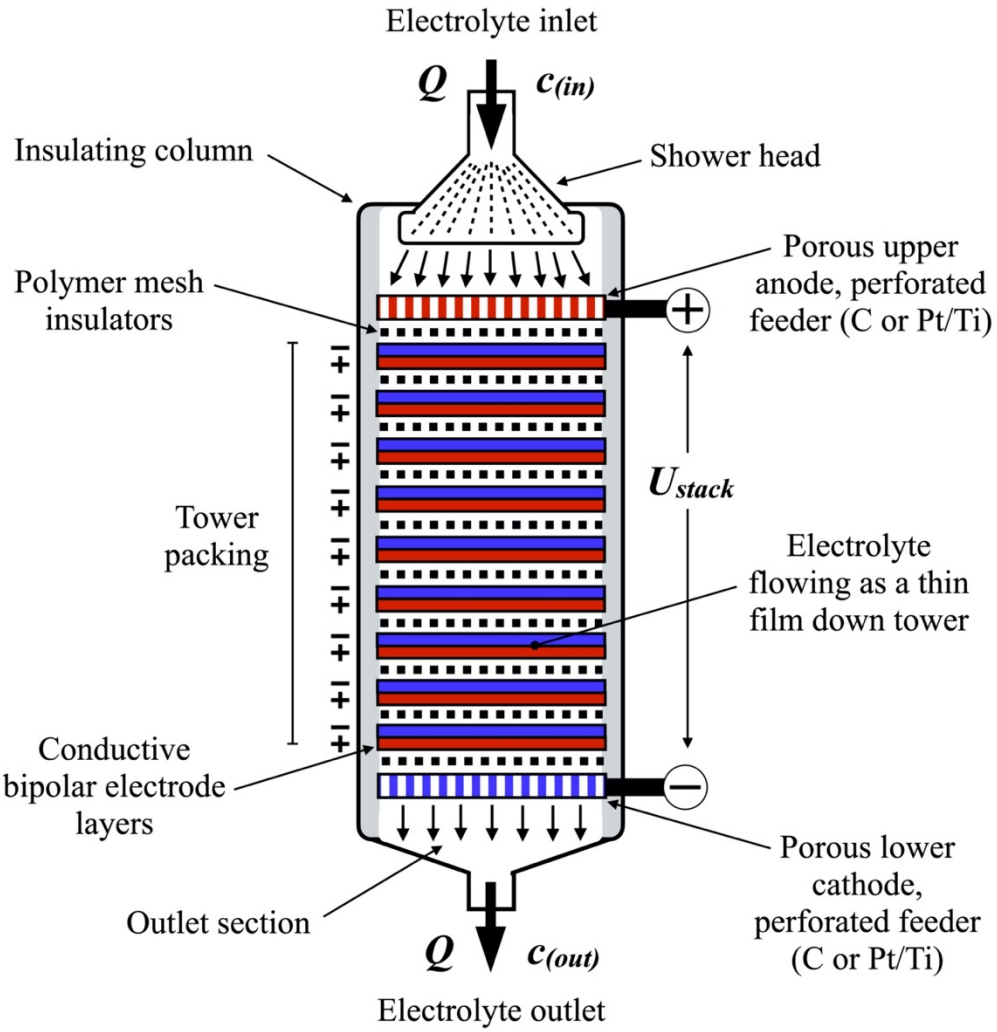
Electrolyte inlet
Q
c(in)
Insulating column
Shower head
Porous upper anode, perforated feeder (C or Pt/Ti)
Polymer mesh insulators
Ustack
Tower packing
Electrolyte flowing as a thin film down tower
Conductive bipolar electrode layers
Porous lower cathode, perforated feeder (C or Pt/Ti)
Outlet section
Q
c(out)
Electrolyte outlet

Fig. 1

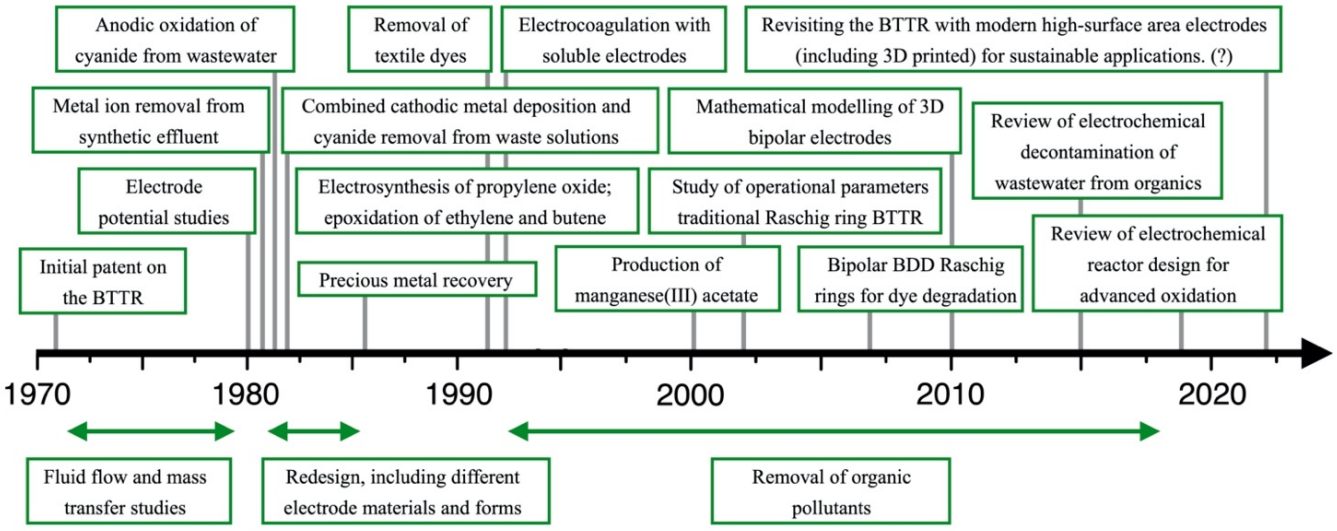
Anodic oxidation of cyanide from wastewater
Removal of textile dyes
Electrocoagulation with soluble electrodes
Revisiting the BTTR with modern high-surface area electrodes (including 3D printed) for sustainable applications. (?)
Metal ion removal from synthetic effluent
Combined cathodic metal deposition and cyanide removal from waste solutions
Mathematical modelling of 3D bipolar electrodes
Review of electrochemical decontamination of wastewater from organics
Electrode potential studies
Electrosynthesis of propylene oxide; epoxidation of ethylene and butene
Study of operational parameters traditional Raschig ring BTTR
Review of electrochemical reactor design for advanced oxidation
Initial patent on the BTTR
Precious metal recovery
Production of manganese(III) acetate
Bipolar BDD Raschig rings for dye degradation
1970
1980
1990
2000
2010
2020
Fluid flow and mass transfer studies
Redesign, including different electrode materials and forms
Removal of organic pollutants

Fig. 2

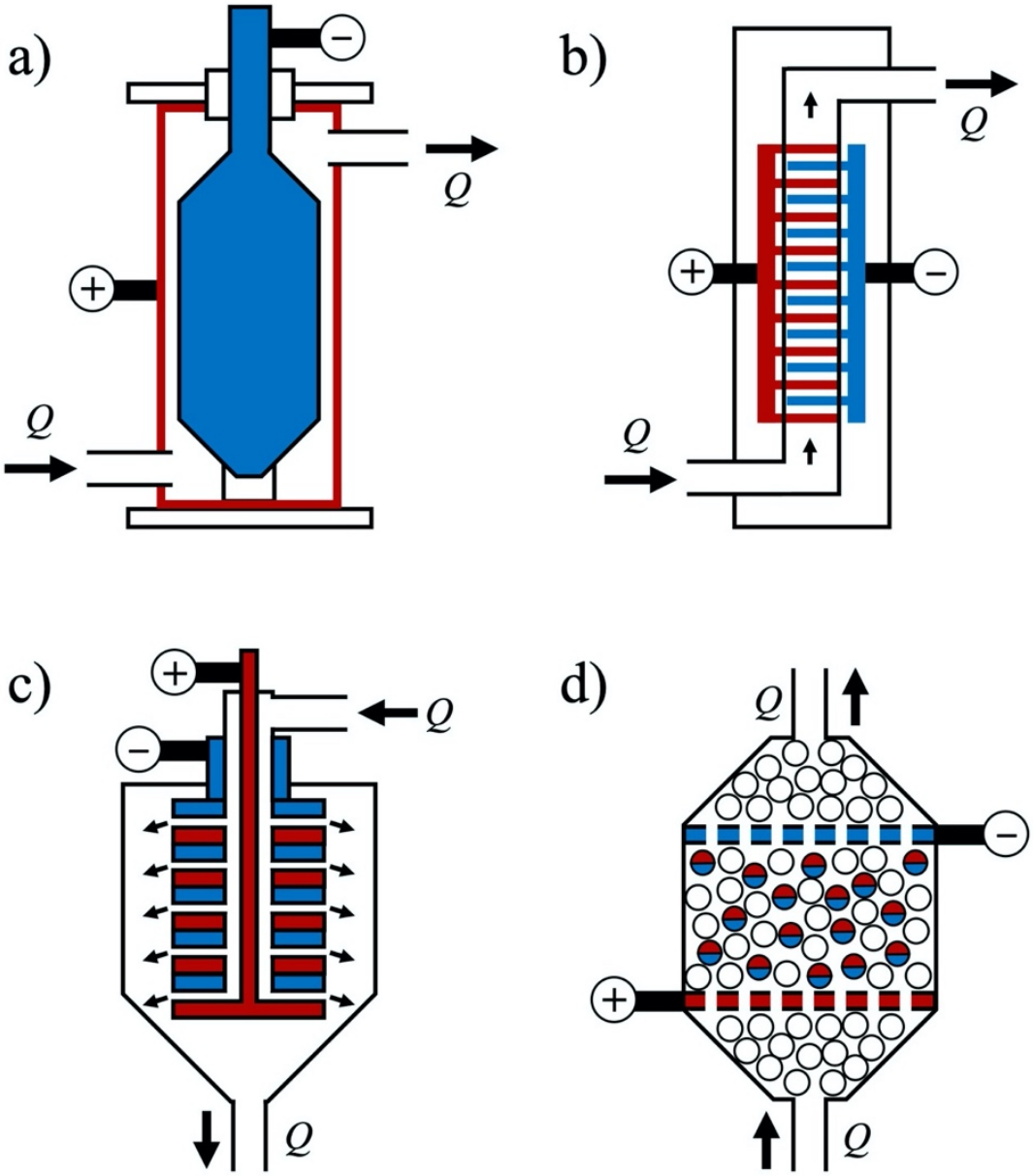

Fig. 3

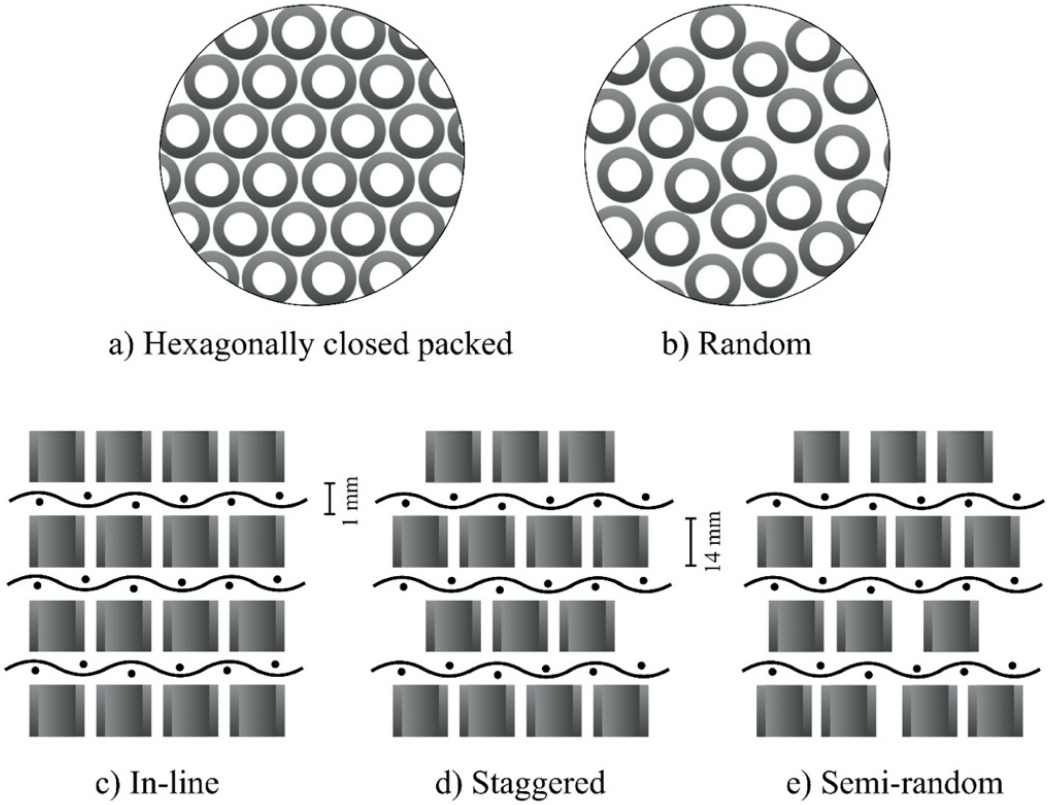
a) Hexagonally closed packed
b) Random
1 mm
14 mm
c) In-line
d) Staggered
e) Semi-random

Fig. 4

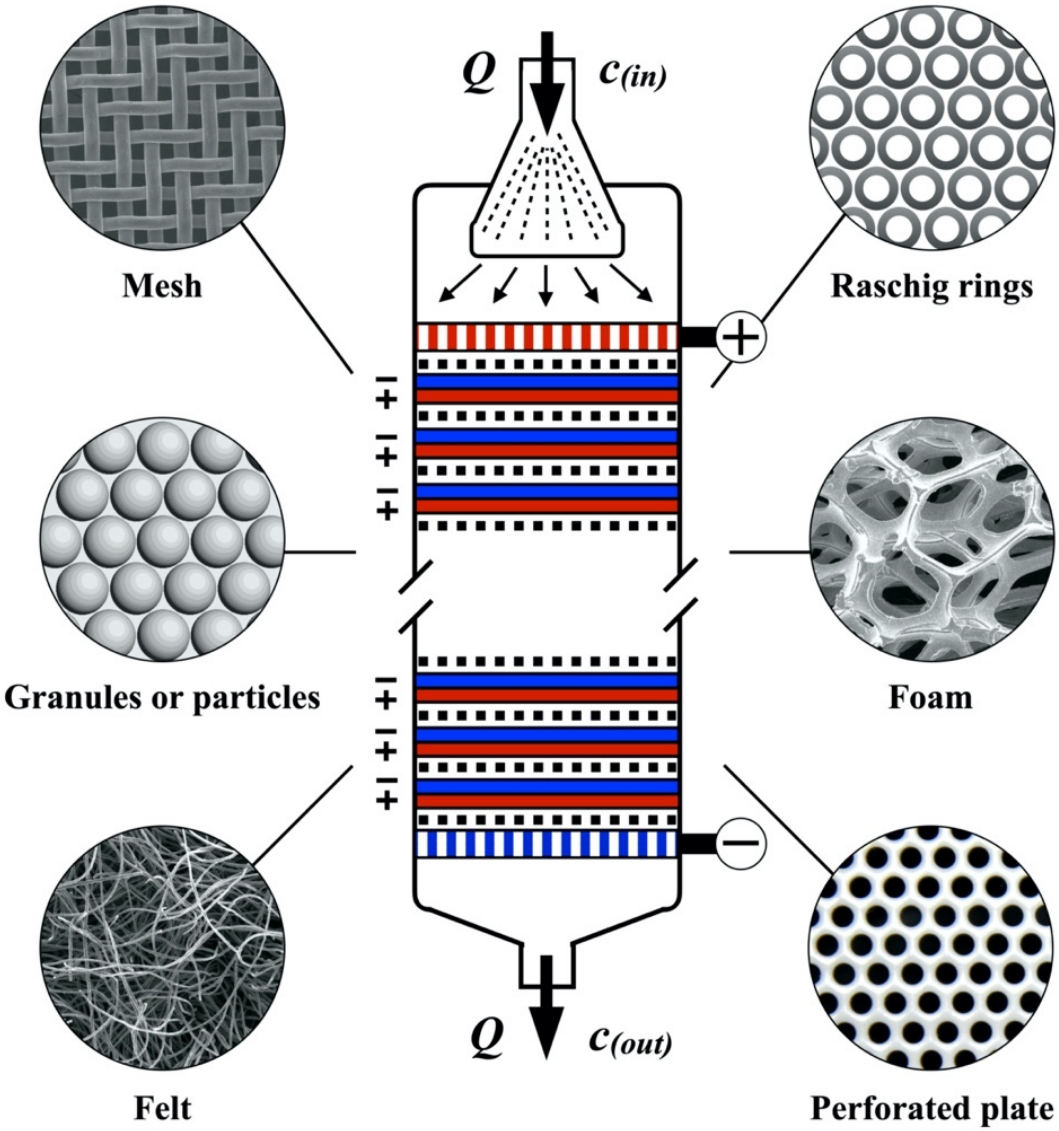
Q
c(in)
Mesh
Raschig rings
Granules or particles
Foam
Felt
Perforated plate
Q
c(out)

Fig. 5

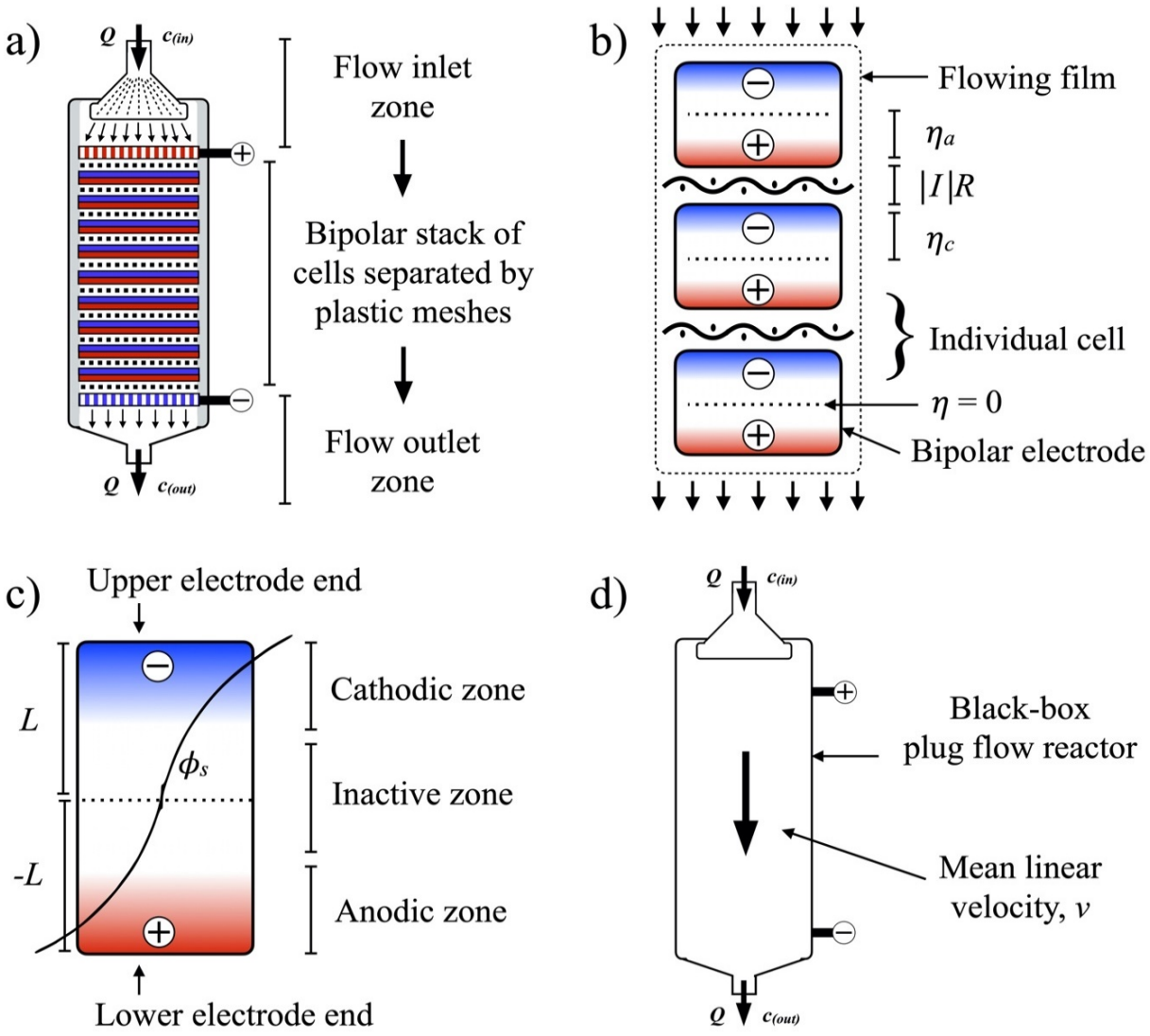
a)
Q
c(in)
Flow inlet zone
Bipolar stack of cells separated by plastic meshes
Flow outlet zone
Q
c(out)
b)
Flowing film
η_a
$|I|R$
η_c
Individual cell
$\eta = 0$
Bipolar electrode
c)
Upper electrode end
L
ϕ_S
-L
Cathodic zone
Inactive zone
Anodic zone
Lower electrode end
d)
Q
c(in)
Black-box plug flow reactor
Mean linear velocity, v
Q
c(out)

Fig. 6

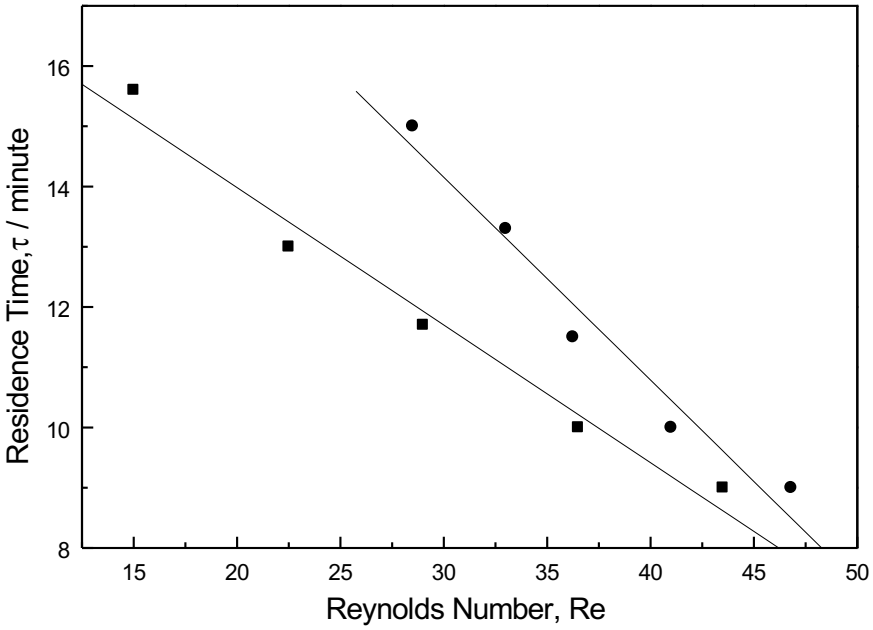
Residence Time, τ / minute
Reynolds Number, Re
16
14
12
10
8
15
20
25
30
35
40
45
50

Fig. 7

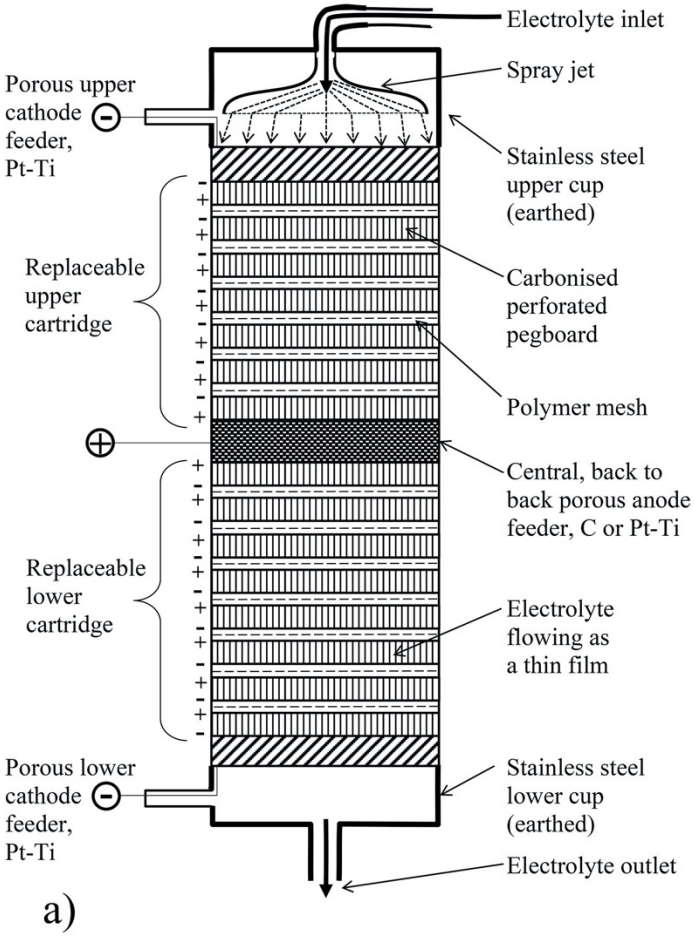
Electrolyte inlet
Spray jet
Porous upper cathode feeder, Pt-Ti
Stainless steel upper cup (earthed)
Replaceable upper cartridge
Carbonised perforated pegboard
Polymer mesh
Central, back to back porous anode feeder, C or Pt-Ti
Replaceable lower cartridge
Electrolyte flowing as a thin film
Porous lower cathode feeder, Pt-Ti
Stainless steel lower cup (earthed)
Electrolyte outlet
a)

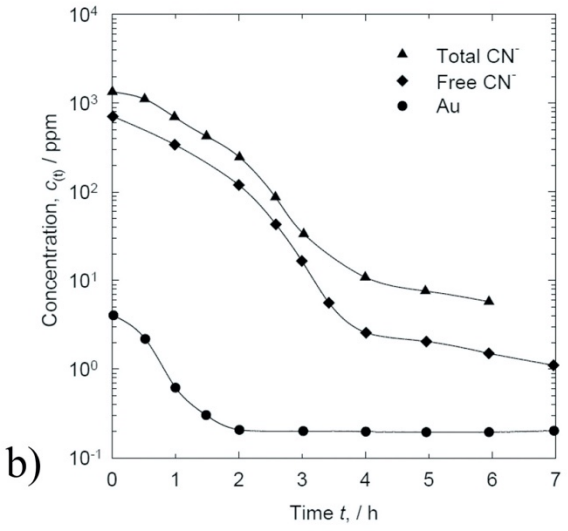
Total CN-
Free CN-
Au
Concentration, $c_{(t)}$ / ppm
Time t, / h
b)

Fig. 8

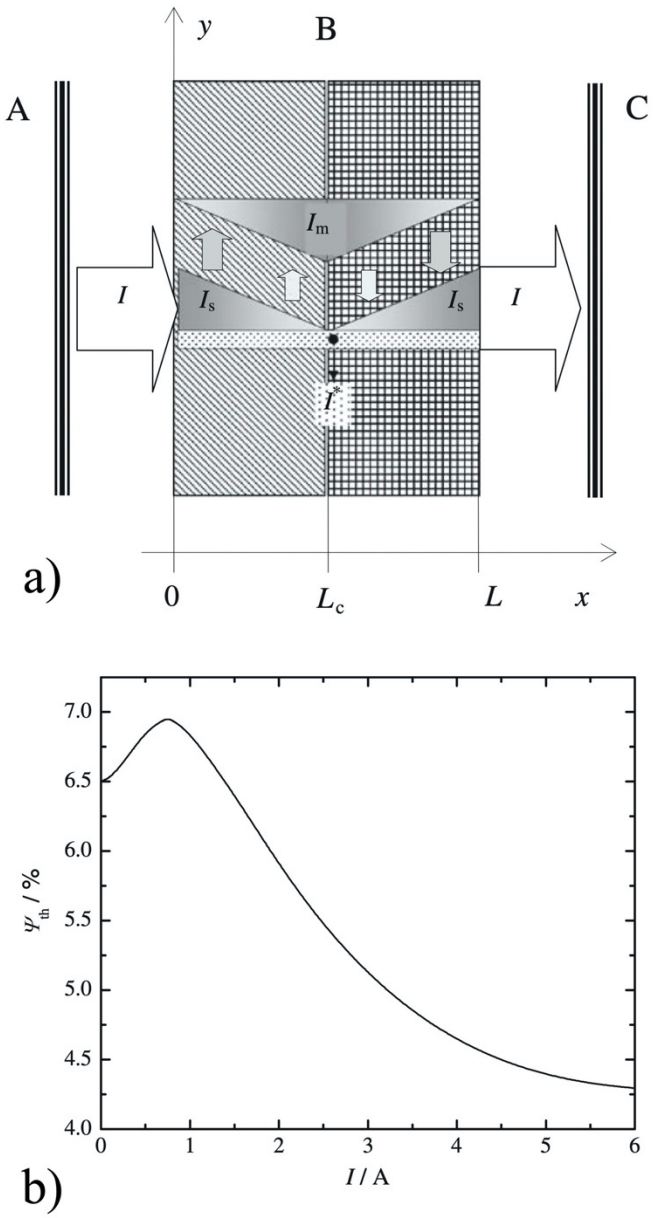

Fig. 9

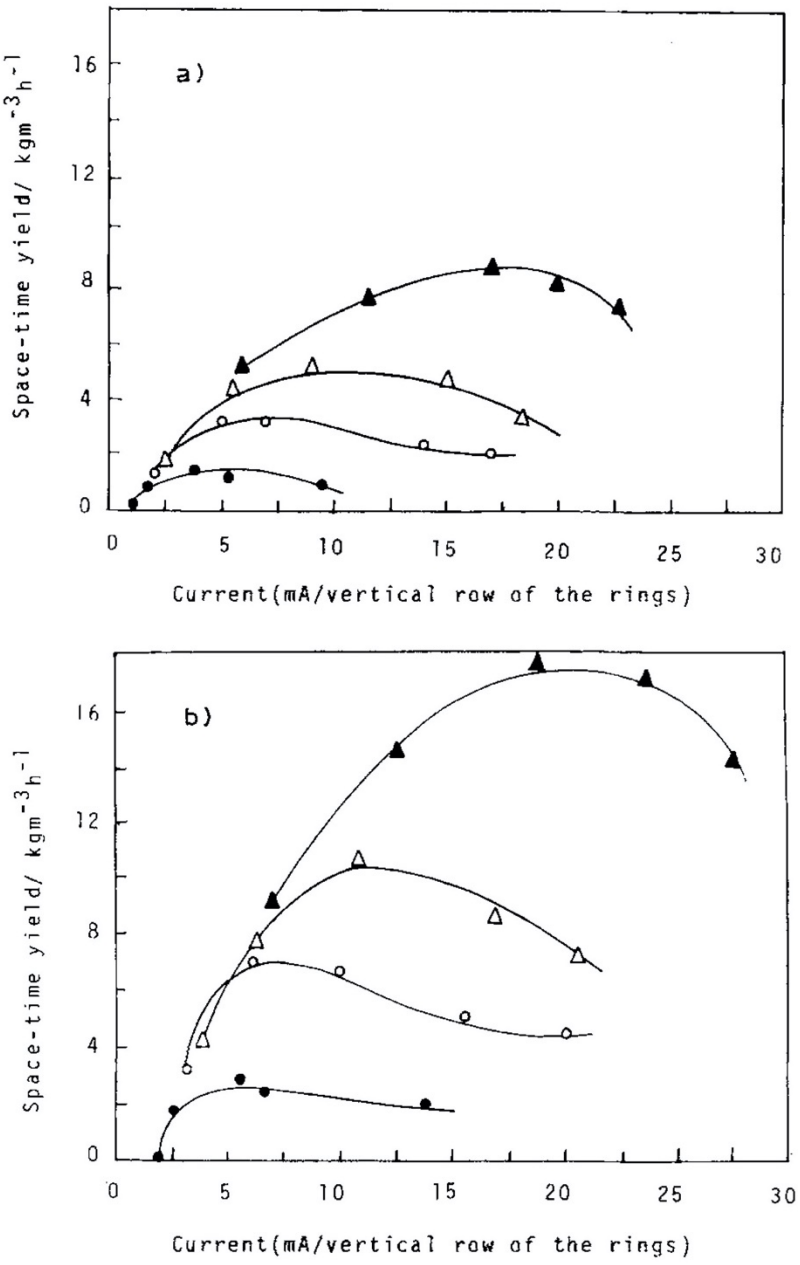
a)
b)
Space-time yield/ kgm^{-3}h^{-1}
Current(mA/vertical row of the rings)
0
4
8
12
16
0
5
10
15
20
25
30

Fig. 10

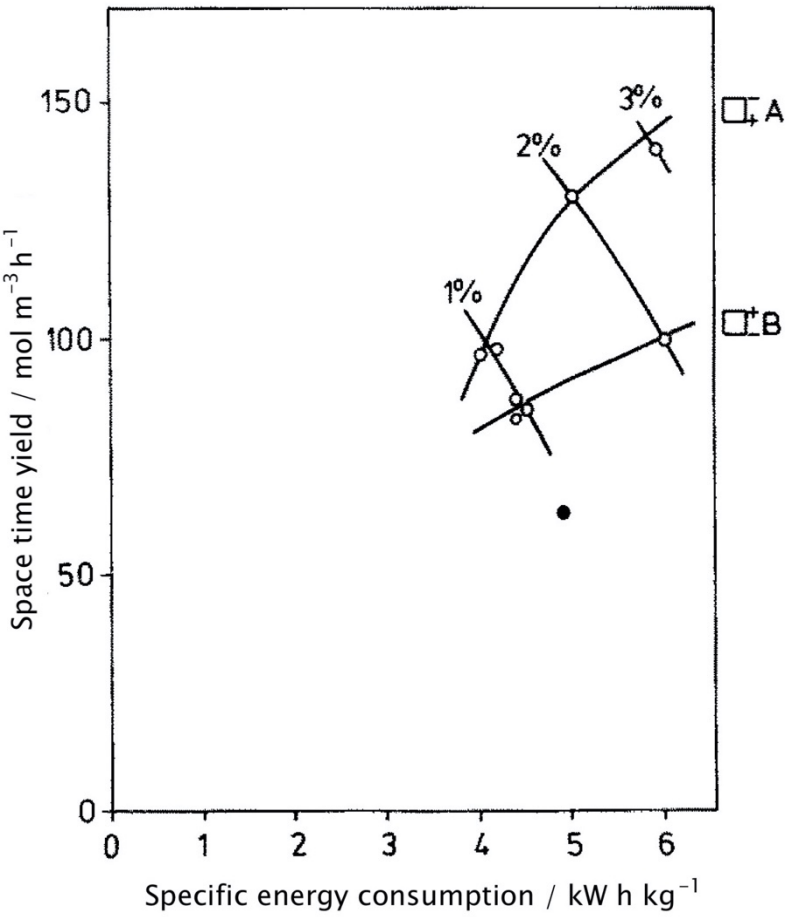
150
100
50
0
0
1
2
3
4
5
6
Space time yield / mol m^{-3} h^{-1}
Specific energy consumption / kW h kg^{-1}
1%
2%
3%
A
B

Fig. 11

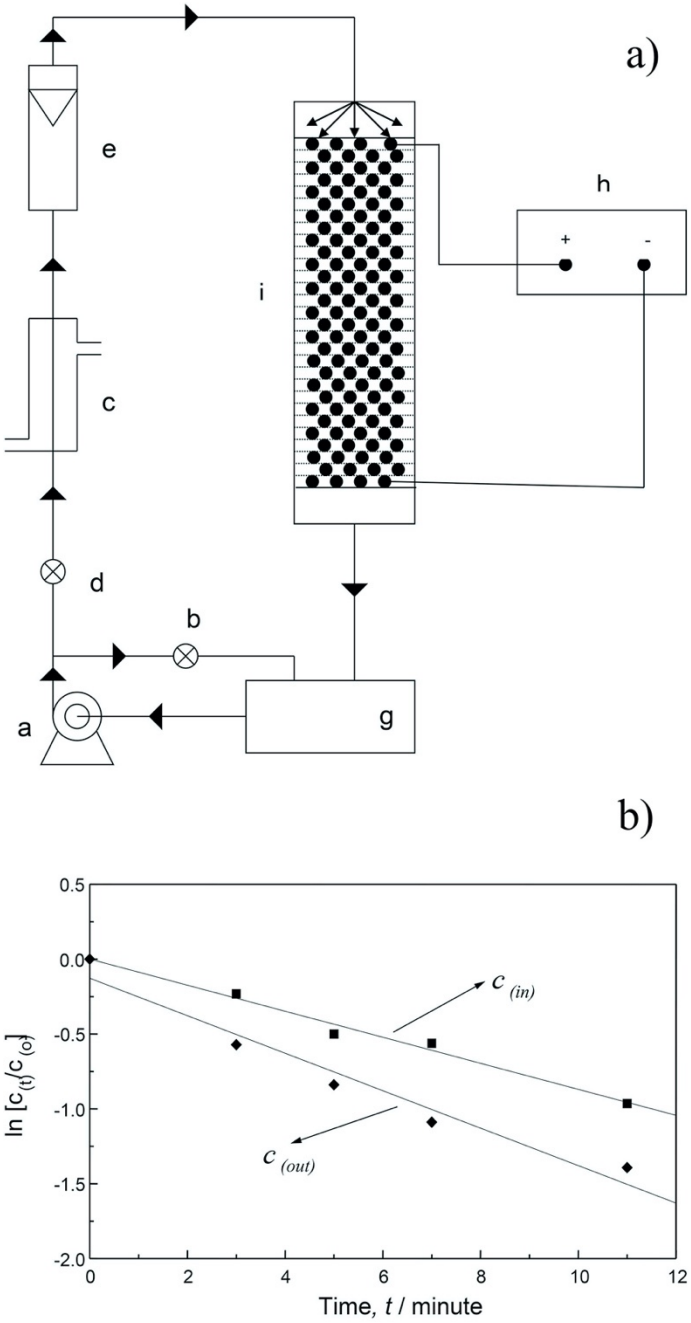
a)
e
h
+
-
i
c
d
b
a
g
b)
0.5
0.0
-0.5
-1.0
-1.5
-2.0
0
2
4
6
8
10
12
ln [c(t)/c(o)]
c (in)
c (out)
Time, t / minute

Fig. 12

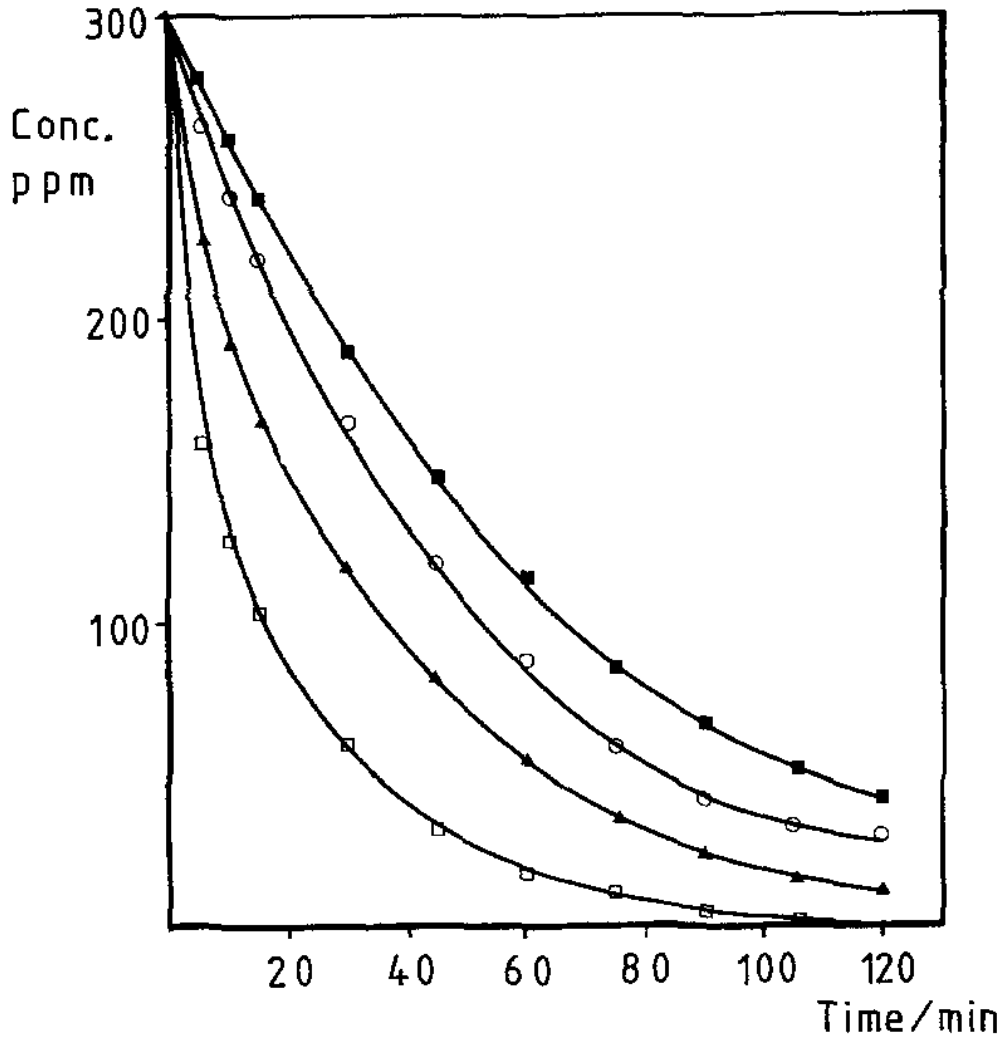

Fig. 13

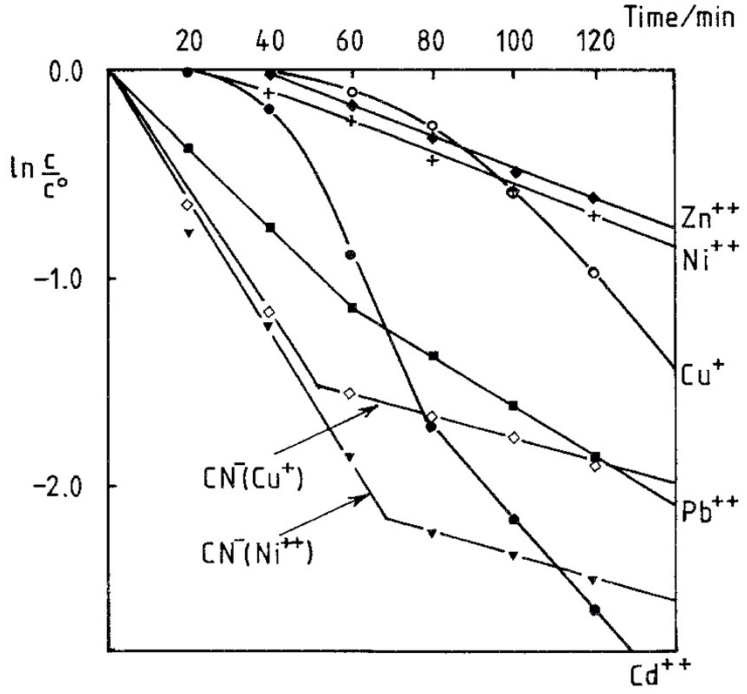

Fig. 14

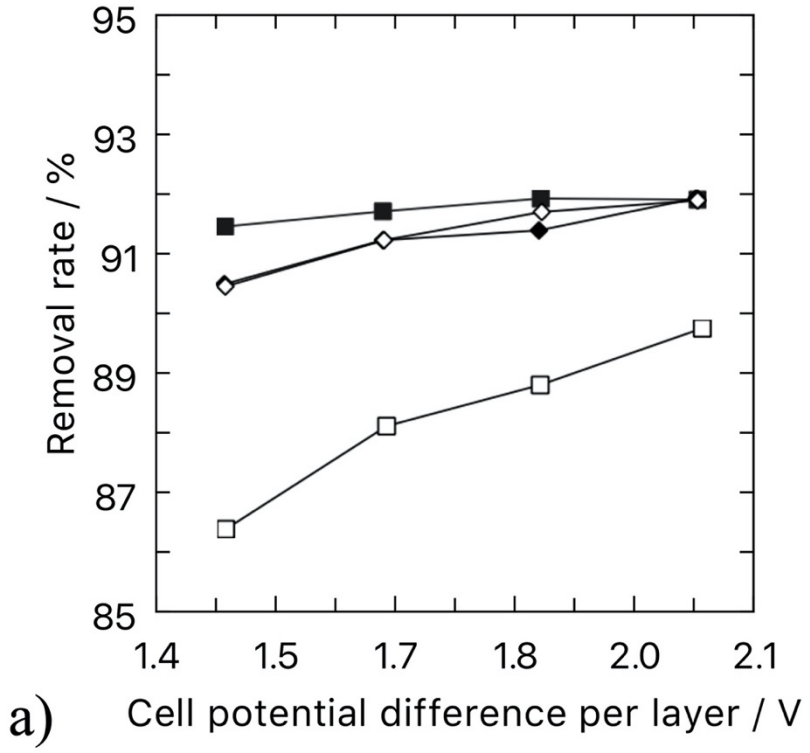
95
93
91
89
87
85
Removal rate / %
1.4
1.5
1.7
1.8
2.0
2.1
a)
Cell potential difference per layer / V

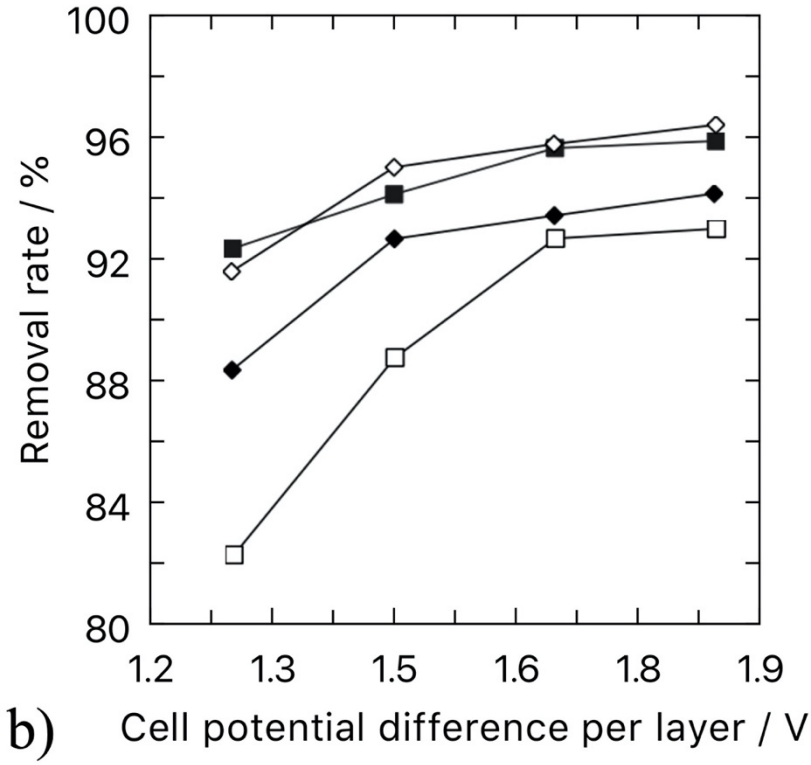
100
96
92
88
84
80
Removal rate / %
1.2
1.3
1.5
1.6
1.8
1.9
b)
Cell potential difference per layer / V

Fig. 15